nature physics

Article

https://doi.org/10.1038/s41567-023-02016-4

Visualizing slow internal relaxations in a two-dimensional glassy system

Received: 13 May 2022

Accepted: 7 March 2023

Published online: 20 April 2023

Check for updates

Yanshuang Chen[1,2], Zefang Ye[1], Kexin Wang[1], Jiping Huang[1], Hua Tong[3], Yuliang Jin[4], Ke Chen[5], Hajime Tanaka[6,7] ✉ & Peng Tan[1,2] ✉

Unlike a crystal, a glassy solid state displays slow internal relaxation processes besides vibrational modes even when structural (α) relaxation is frozen. The precise nature of such residual local relaxation modes remains poorly understood due to the lack of real-space information. Here we directly visualize the internal relaxations in a glass via a long-time observation of the dynamics of a mechanically driven two-dimensional granular system that shows a pinning-induced transition. This allows directly visualizing the internal relaxations in a glass. On approaching the glass transition, vanishing cage-breaking motion is observed, accompanied by the emergence of a restricted dynamic mode characterizing slow β relaxation. The emergence of bond rigidity freezes the structure relaxation and leads to slow β motion. Our findings indicate that unlike crystallization, where all the bonds are constrained, vitrification in a disordered system freezes α relaxation and accompanies elastic percolation, but the remaining non-constrained bonds provide room for slow β relaxation.

When a liquid crystallizes, all the relaxational modes except for the vibrational phonon modes are frozen. In contrast, not all the relaxational modes of motion are frozen in a glass state despite being solid. In practice, besides the ultraslow α relaxation responsible for the solidity, the glassy state also exhibits subtle slow internal relaxations, known as the slow β (or Johari–Goldstein) mode. This mode is a manifestation of the structural complexity intrinsic to disordered systems and the non-equilibrium nature of a glassy state[1–6]. Unlike the fast β relaxation process, identified as the rattling motion inside the cage formed by neighbouring particles, the microscopic nature of the slow β relaxation process remains elusive despite it being widely observed in glassy materials.

Since the pioneering work of Johari and Goldstein, slow β relaxation has been extensively studied in polymetric, organic, ionic, metallic and atomic glasses by various experimental methods, such as dielectric spectroscopy, dynamic mechanical spectroscopy, nuclear magnetic resonance, quasi-elastic nuclear resonant scattering[7] and dynamic light scattering[8]. It appears as a secondary peak or a high-frequency excess wing of the α peak in the imaginary part of the dielectric relaxation spectra. Various interpretations of this relaxation mode have been proposed, including the intramolecular motion for polymer glasses[9], restricted molecule reorientation for organic glasses[10–12] and string-like translational motion for metallic glasses[13–16]. However, it was also suggested that the dominant slow internal dynamics belongs to early α relaxation, that is, extended or localized hopping motion in soft spots for model glass systems[4,6,17] and T1-topological excitation for soft biological glasses[18,19], serving as the precursors of α relaxation and showing further slowing down deep in a glass state. Various theoretical ideas have also been proposed to explain slow β relaxation, but without consensus. They include the cooperative process of motions coupled together by interparticle interactions in the coupling model[20], the low-energy part of α relaxation in the random first-order transition theory[1], the precursor of α relaxation through dynamic facilitation[21,22], the motions associated with the Gardner-like transition[3,23–25] and the

[1]State Key Laboratory of Surface Physics and Department of Physics, Fudan University, Shanghai, China. [2]Institute for Nanoelectronic Devices and Quantum Computing, Fudan University, Shanghai, China. [3]Department of Physics, University of Science and Technology of China, Hefei, China. [4]Institute of Theoretical Physics, Chinese Academy of Sciences, Beijing, China. [5]Institute of Physics, Chinese Academy of Sciences, Beijing, China. [6]Research Center for Advanced Science and Technology, University of Tokyo, Meguro-ku, Japan. [7]Department of Fundamental Engineering, Institute of Industrial Science, University of Tokyo, Meguro-ku, Japan. ✉e-mail: tanaka@iis.u-tokyo.ac.jp; tanpeng@fudan.edu.cn

restricted reorientation motion within metastable islands[11]. Thus, we may say that the origin of slow and subtle internal relaxations in a glassy system has remained unclear despite intensive research.

Such a diversity of interpretations may come from the difficulty in microscopically accessing such subtle intermediate motion. Due to the slow and subtle nature of the slow β mode, its observation requires precise isolation from both fast β and slow α modes, whose timescales are separated by many orders of magnitude. However, experimentally accessing subtle particle motions in real space over such a vast timescale in a glassy state is highly challenging.

To overcome this difficulty, we specially designed a two-dimensional (2D) binary granular system composed of magnetic discs, enabling precise measurements of tiny structure adjustments over an ultralong time. Instead of changing the particle density, we introduce a random particle pinning to this system to induce glass transition in a controlled manner[26–32]. We excite particle motion by applying a small-enough volumetric mechanical perturbation, mimicking thermal excitation at low temperatures. This system allows probing the relaxation dynamics from close to glass transition to deep in a glass state. We confirm that flow-like particle motion becomes increasingly difficult to occur and eventually frozen at the glass transition with increasing fraction of pinned particles c. This ceasing of cage-breaking motion is accompanied by the emergence of a restricted dynamic mode characterizing the slow β relaxation. We find that the emergence of bond rigidity leads to the freezing of structure relaxation and the activation of slow β motion.

Results

Model granular system and its characterization

The details of our experimental setup are as follows. We confine a binary mixture of magnetic discs (diameter, $d_{large} = 10.00 \pm 0.10$ mm, $d_{small} = 7.00 \pm 0.10$ mm, height $h = 2.00 \pm 0.05$ mm, number ratio N_{large}:N_{small} = 1:1) in a 2D plane at an area fraction of 12% (Fig. 1a). The discs interacting with the repulsive pair interaction in the confining plane, $U(r) \approx r^{-3}$, form an amorphous solid state without any direct particle–particle contacts (Extended Data Fig. 1a). The particle–wall (smooth) static friction coefficient is around $\mu_s \approx 0.1$, and the resulting friction force f_{fri} is about 0.25% of the repulsive force f_{sys} acting between the particles. We designed a special mechanical perturbation setup, which applies a perturbation to each particle of the upper 2D sample through attractive magnetic interactions by moving a bottom plate (velocity V) to which magnetic discs (interparticle distance D) are fixed. The mechanical perturbation strength $\langle f_p \rangle$ is adjusted by the vertical distance h_1 to the sample plate. A small-enough perturbation strength ($f_{fri} < f_p \ll f_{sys}$) effectively acts as thermal excitation typical to a low temperature. Thus, we set the mechanical perturbation strength to be the effective temperature corresponding to a thermal system slightly above the glass transition.

To study glass transition in this system, we introduce particle pinning under the above fixed strength of mechanical perturbation (that is, at the fixed effective temperature). We pin a small number of particles randomly chosen from a configuration relaxed for a long-enough time (Fig. 1a). This procedure allows us to realize a pinning-induced glass transition by changing the fraction of pinned particles[4,26–32]. With this pinning method, we can probe the relaxation dynamics from slightly above the glass transition to deep in a glass state.

Here we define the key timescales to describe the relaxation dynamics in our experiments. Furthermore, $\tau_0 \approx D/V$ is the average interval of particle collisions induced by the perturbation from the moving bottom plate, and τ_s (usually set as $\tau_s \approx 2 \times 10^3 \tau_0$) is the duration of continuous mechanical perturbation in the unit of τ_0. Within τ_s, particle movement is restricted in a small basin of the potential energy landscape (PEL). For example, as shown in Fig. 1b, the system behaves as a solid, as evidenced by the three-decade plateau in the mean square displacement (MSD), $\langle \Delta r^2(t)/a^2 \rangle$, where time t is in units of τ_0 and a is the average interparticle distance. After a time interval of τ_s, we take the bottom plate away and record the static configuration locked by the tiny wall–disc friction (0.25% of the repulsive force between the particles). This state is very close to the minima of the system's PEL in the absence of friction. This unique procedure mimics a 'perturbation-lock' procedure (Fig. 1d(i),(ii)). We repeat this procedure another 1,000 times to follow the particle-level dynamics. Thus, we experimentally follow the ultralong-time relaxation dynamics with high accuracy, using τ_s as the primary time unit. We note that we can carefully adjust the perturbation strength such that the α-relaxation time at $c = 0$ is a bit longer than $10^6 \tau_0$, which is comparable with the relaxation time of a deeply supercooled liquid near the glass transition in previous simulations[21,22,26,33]. As an example, we show the dynamics at a high perturbation strength (Extended Data Fig. 1b).

As evidenced by the long-time MSD behaviours ($\langle \Delta r^2(t)/a^2 \rangle$) (Fig. 1c), which covers a 10^3 times longer time than that shown in Fig. 1b, as the pinning fraction c increases, the long-time relaxation dynamics ($\Delta t \approx 500\tau_s \approx 10^6 \tau_0$) changes from α-type slow diffusion (MSD approaches 0.5×10^{-1}) at $c \leq 1.2\%$ to small-amplitude, extremely slow subdiffusion (a factor of 100 reductions of MSD) at $c \approx 3.6\%$. Thus, increasing the pinning fraction c brings the system to a glass state, that is, induces the glass transition[4,26].

Interestingly, the small-amplitude structure adjustments in our system are different from the trivial liquid-like diffusion and pure vibrations. They are characterized by a hierarchical character with multiple-length-scale particle movements, shown via the schematic of the PEL picture (Fig. 1d). During $10^3 \tau_s$ at $c \leq 3.0\%$, we can find two types of particle movement. One is a cage-breaking-type particle movement (typically, $\Delta r \geq 0.3a$) that constitutes the lowest-energy part of α relaxation[1]. The other is much-smaller-amplitude particle jumps ($\Delta r \approx 0.1a$; either coupled or not coupled with cage-breaking motion) that correspond to barrier crossings between shallow basins of the PEL, that is, local-bond-breaking motion (Fig. 1d(iii)). The large cage-breaking-type movement ($\Delta r \geq 0.3a$) vanishes at around $c^* \approx 3.0\%$, whereas the smaller jumps ($\Delta r \approx 0.1a$) still occur even at $c > c^*$ (Fig. 1d(iii),(iv)). Thus, we determine the pinning-induced glass transition point as $c^* \approx 3.0\%$ above which internal non-diffusive modes dominate the slow relaxation. This identification is further supported by the particle-level Van Hove correlation function[34], namely, $G_{s,i}(r, t)$, for a group of particles i that have a narrow range of $\langle \Delta r^2(t) \rangle$ ($\Delta t = 500\tau_s$). The long-time motion of the fastest particles forms a second peak or shoulder at a characteristic moving distance (Extended Data Fig. 1c–e).

Here we note that our system is confined by a rigid circular wall, and the circular wall reduces the amplitude of nearby particle motions through a short-range layering effect (Extended Data Fig. 2a–e). However, we find that the wall does not change the glass transition point c^*; instead, the transition is more distinct for layers close to the wall, which suggests that the wall changes the fragility of the transition alone but not the glass transition point[35].

Classification of elementary particle rearrangements

Interestingly, we find that the dominant jump-like internal structure relaxation, such as cage-breaking and local-bond-breaking processes, occurs in the form of the so-called T1 events[18] (known as the shear transformation zone). A T1 event is a primary type of structural adjustment of four neighbouring particles $\{h, k, m, n\}$ that accompanies a topological change for the two diagonal bonds, as illustrated by the four-particle tetragon's Voronoi tessellation (Fig. 2a–d, insets). The short bond $\{h, k\}$ becomes the long bond, and the long bond $\{m, n\}$ becomes the short bond after the event. We characterize the amplitude of a T1 event by l_{sl}, which is the time average of the normalized difference between the long diagonal length l_{long} and short diagonal length l_{short} of the T1 tetragon, namely, $l_{sl} = \langle (l_{long} - l_{short})/l_{long} \rangle$ (note that particle i may have two values of $l_{sl}(i)$ if it is involved in two different T1 events). Here we note that the 'bonds' we defined here are from the neighbour analysis

https://doi.org/10.1038/s41567-023-02016-4

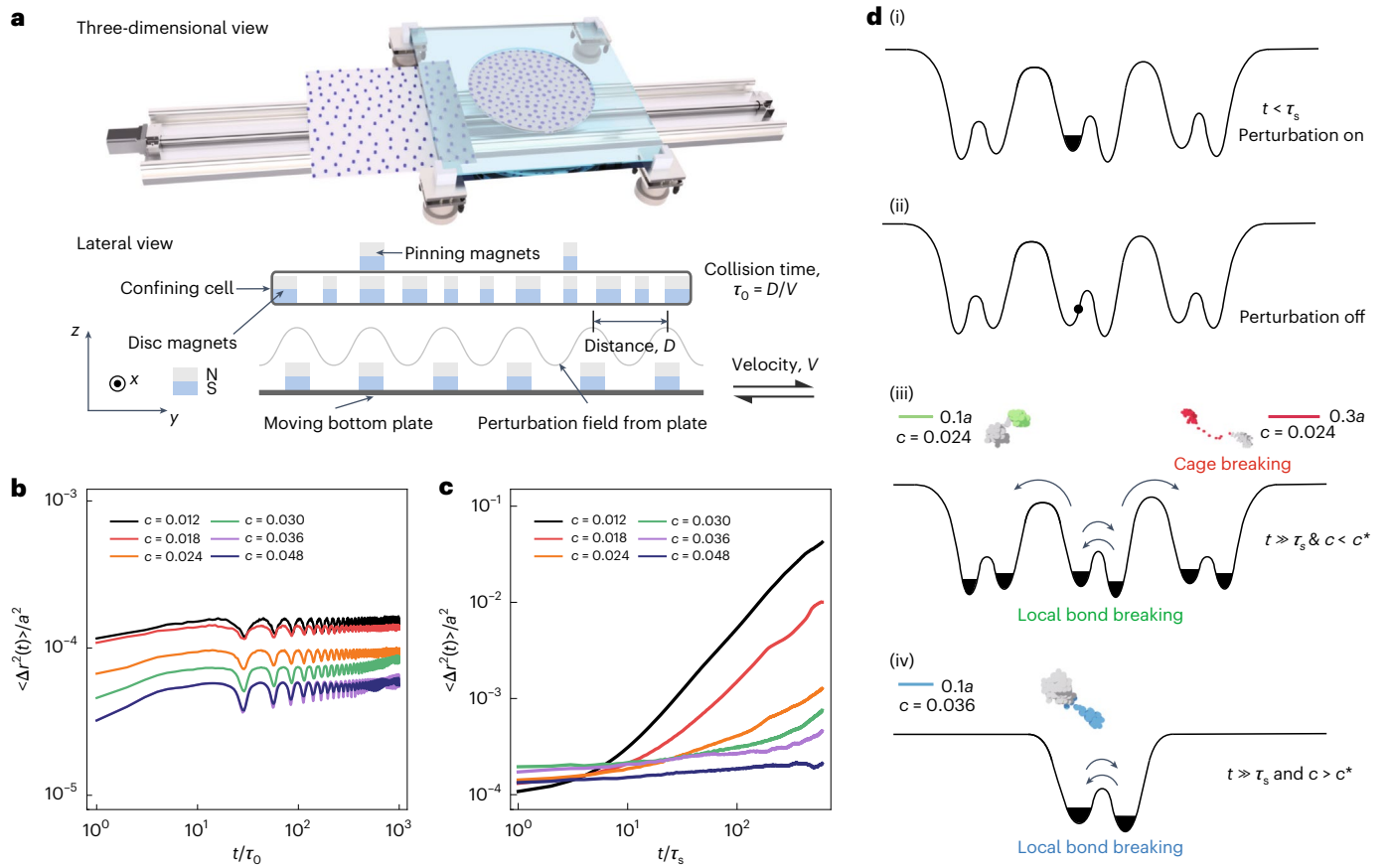

Fig. 1 | Experimental details and reduction in internal structure relaxation across a pinning-induced glass transition. a, Experimental setup. Bidisperse magnetic discs interacting with a long-range repulsion ($U(r) \approx r^{-3}$) form an amorphous solid state under 2D confinement in the upper layer. A periodically moving bottom plate with disc magnets applies a suitably, sufficiently small mechanical perturbation to each particle in the upper layer that mimics thermal agitation. The particle–wall friction force f_{fri}, perturbation force f_p and particle–particle interaction force f_{sys} in the sample satisfy the relation of $f_{fri} < f_p \ll f_{sys}$. Changing the pinning density, we control the relaxation dynamics from slightly above the glass transition to very deep in a glass state. Here τ_0 is the characteristic interval of 'collision' due to perturbation and τ_s is the duration of periodic perturbation in the unit of collision interval (usually, $\tau_s \approx 2 \times 10^3 \tau_0$). After a time duration of τ_s, we take the bottom plate away and record the static configuration that is locked by the tiny particle–wall friction. This unique procedure mimics a 'perturbation-lock' procedure, and we repeat this procedure for another three decades. **b**, Typical MSDs of $\langle\Delta r^2(t)\rangle/a^2$ of our pinning samples within τ_s. The plateau has a very small value (around 10^{-4}), which is kept over three decades within τ_s. **c**, Typical long-time MSD over $10^3\tau_s$. The long-time relaxation dynamics changes from diffusive to solid-like with an increasing pinning fraction c. **d**, Schematic of the relaxation dynamics across the pinning-induced glass transition from the PEL perspective. Three typical particle trajectories during $10^3\tau_s$ are shown in (iii) and (iv).

using Voronoi methods, different from chemical bonds with specific energy and length.

For all the observed T1 events occurring below and above the pinning-induced glass transition, the relation between the amplitude of a T1 event (l_{sl}) and the particle's moving distance ($\Delta r(i)$) during the event can be unified into a single master curve with some scatter for $c \approx 1.2\%$, $c \approx 2.4\%$, $c \approx 3.6\%$ and $c \approx 4.8\%$ (Fig. 2a–d, respectively). We also show another representation using the particle's total displacement ΔR ($\Delta R = \Sigma_{i=\{h,k,l,m\}}|\Delta \mathbf{r}(i)|$) for a tetragon (Extended Data Fig. 3a–d).

Based on the correlation among $l_{sl}(i)$, $\Delta r(i)$ and the number of neighbour changes during the T1 event, $N_b(i)$, we can classify T1 events into two types: one type is large-ratio T1 events responsible for cage breaking ($l_{sl} \geq 0.2$, $\Delta r \geq 0.3a$; particle jump involves at least two T1 events), which are active only above the glass transition point (that is, for $c \leq c^*$), as shown in Fig. 2a ($c \approx 1.2\%$) and Fig. 2b ($c \approx 2.4\%$). The other type is small-ratio T1 events responsible for local bond breaking ($l_{sl} < 0.2$, $\Delta r < 0.3a$ and $N_b(i) \leq 1$), which are active above the glass transition point (that is, for $c \leq c^*$) (Fig. 2a,b) and remain prevalent even below the glass transition point (that is, for $c > c^*$) (Fig. 2c ($c \approx 3.6\%$) and Fig. 2d ($c \approx 4.8\%$)). Note that the blue symbols (Fig. 2, $N_b(i) \approx 0$) represent reversible T1 events that are responsible for a reversible bond break, and the reversibility becomes the dominant feature of T1 events for $c > c^*$. The systematic change in the master curves with increasing pinning fraction c (Fig. 2a–d) suggests that the reduction in internal relaxation is a consequence of eradicating large-ratio T1 events, as supported by the cluster analysis of the two types of T1 event for all the samples with reducing $\langle\Delta r^2(t)/a\rangle$ (Extended Data Fig. 3e–g). These results indicate that the glass transition is accompanied by the change in a T1-event type from the cage-breaking to local-bond-breaking-only type.

Now, we focus on the characteristics of the two types of T1 event. Large-ratio T1 events usually occur cooperatively, causing a string-like, cooperative jump motion of fast-moving particles (Fig. 2f, orange particles; $\Delta t \approx 10^3\tau_s$); the string's neighbouring particles (blue particles) experience fewer neighbour changes and show smaller jumps. The elementary excitation of this type of motion[1,36] corresponds to a single cage-breaking event (Fig. 2f), which serves as the precursor of a compact slowly flowing cluster (Fig. 2e, red, orange and green particles; $\Delta t \approx 10^3\tau_s$). This process can also be seen from the temporal change in the T1-event frequency (Extended Data Fig. 3h; $c \leq c^*$). A compact cluster exhibiting α-type relaxation (Fig. 2e) is created by a sequential occurrence[21,22] of several elementary large-ratio T1 excitations

https://doi.org/10.1038/s41567-023-02016-4

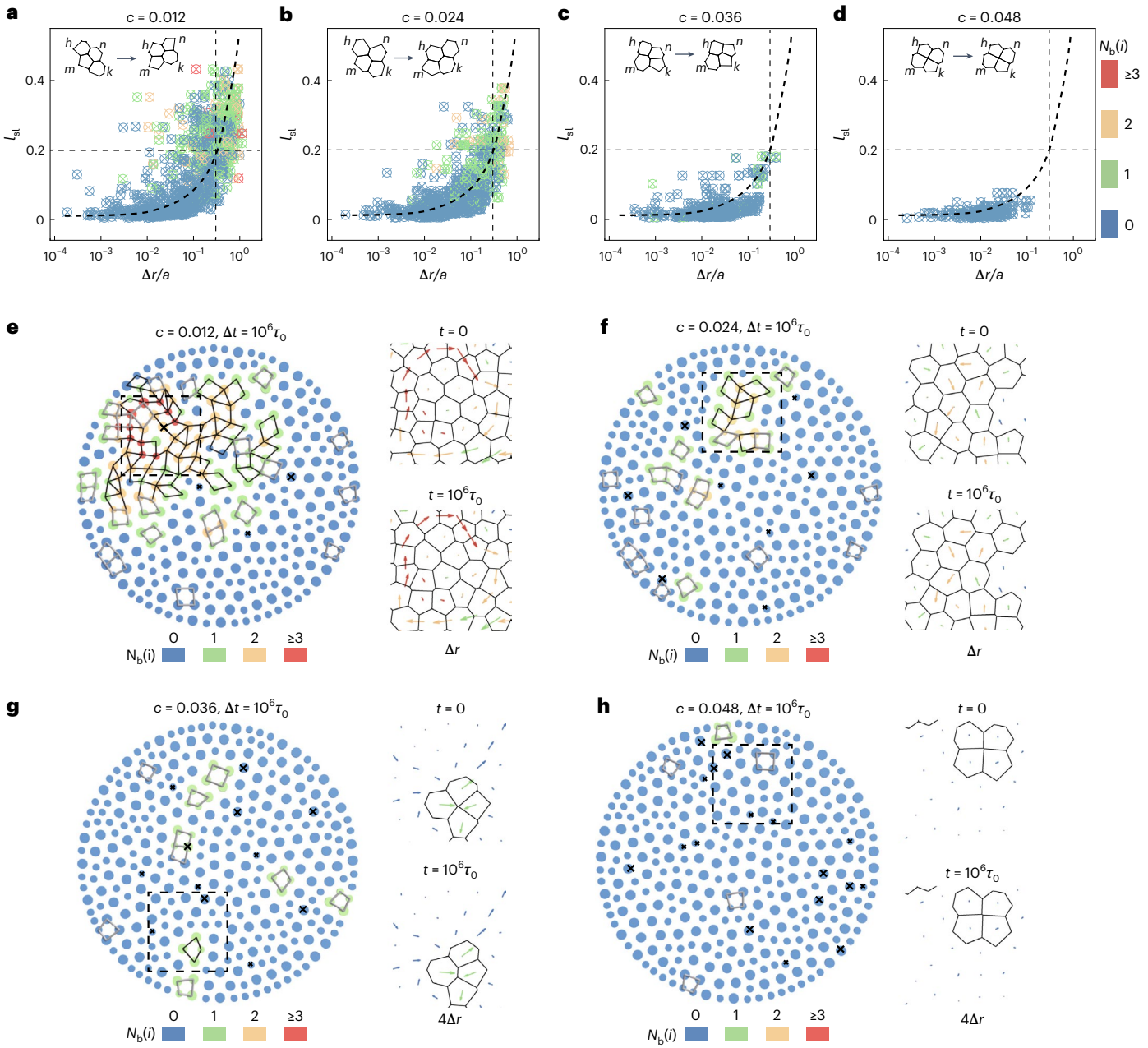

Fig. 2 | Pinning-fraction dependence of the internal relaxation dynamics profiles. a–**d**, Unified Δr–l_{sl} relation of T1 events ($c \approx 1.2\%$ (**a**); $c \approx 2.4\%$ (**b**); $c \approx 3.6\%$ (**c**); $c \approx 4.8\%$ (**d**)). The largest T1 event in each panel is shown in the inset. The T1 events are classified into two types based on the correlation among $l_{sl}(i)$, $\Delta r(i)$ and $N_b(i)$: one is large-ratio T1 events responsible for cage breaking ($l_{sl}(i) \geq 0.2$, $\Delta r(i) \geq 0.3a$; particle jumps involve at least two T1 events), which are only active at $c \leq c^*$ (**a**,**b**). The other is small-ratio T1 events responsible for local bond breaking ($l_{sl}(i) < 0.2$, $\Delta r(i) < 0.3a$ and $N_b(i) \leq 1$), which are also active at $c \leq c^*$ (**a**,**b**) and further prevalent even at $c > c^*$ (**c**,**d**). Note that the blue symbols ($N_b(i) \approx 0$) represent reversible T1 events. The unified master curve (black dotted line) in **a**–**d** suggests a close relation of the internal relaxation reduction with the eradication of large-ratio T1 events with increasing pinning, which changes the character of T1 excitation from 'cage breaking' to 'locally bond breaking'. **e**–**h**, Spatial illustration of the relaxation dynamics ($\Delta t \approx 10^3\tau_s$) with $\Delta \mathbf{r}(i)$ (arrow length and direction), $l_{sl}(i)$ (black and grey tetragons representing large-ratio and small-ratio T1 events, respectively) and $N_b(i)$ (colours of the particles and their displacements) for α-type relaxation (**e**; $c \approx 1.2\%$), cage-breaking relaxation (**f**; $c \approx 2.4\%$), relaxation just approaching a glass state (**g**; $c \approx 3.6\%$), and local and reversible bond-breaking relaxation (**h**; $c \approx 4.8\%$). Voronoi cells of the particles with $N_b(i) > 0$ at $t = 0$ (top) and $t = 10^3\tau_s$ (bottom) are shown in each panel of $\Delta \mathbf{r}(i)$. Accumulation of sequential cage-breaking events forms an α-type relaxation cluster in **e**. A string-like single cage-breaking event is formed by spatially extended large-ratio elementary T1 events (black tetragons) in **f** (the large red and orange arrows pointing to the edge of the Voronoi cells at $t = 0$), and the excitation of this type serves as a precursor of α relaxation (**e**). Small-ratio T1 events (grey tetragons) are localized and can persist into the glass state (**g**,**h**). The displacement fields in **g** and **h** are magnified four times.

(Extended Data Fig. 4a). Note that the string-like elementary excitation can also develop into a string-like larger cluster at a similar pinning fraction (Extended Data Fig. 4e). In contrast, small-ratio T1 events only cause localized neighbour changes, that is, reversible bond-breaking motions (Fig. 2g,h; $\Delta t \approx 10^3\tau_s$). Thus, a large-ratio T1 event is a distinct sign of cage breaking, allowing us to classify the state of a system into the slowly flowing state ($c \leq c^*$) or glass state ($c > c^*$) by the presence or absence of large-ratio T1 events, respectively. For $c > c^*$, we also see further slowing down of small-ratio T1 event excitation with increasing pinning fraction (Extended Data Fig. 3i).

https://doi.org/10.1038/s41567-023-02016-4

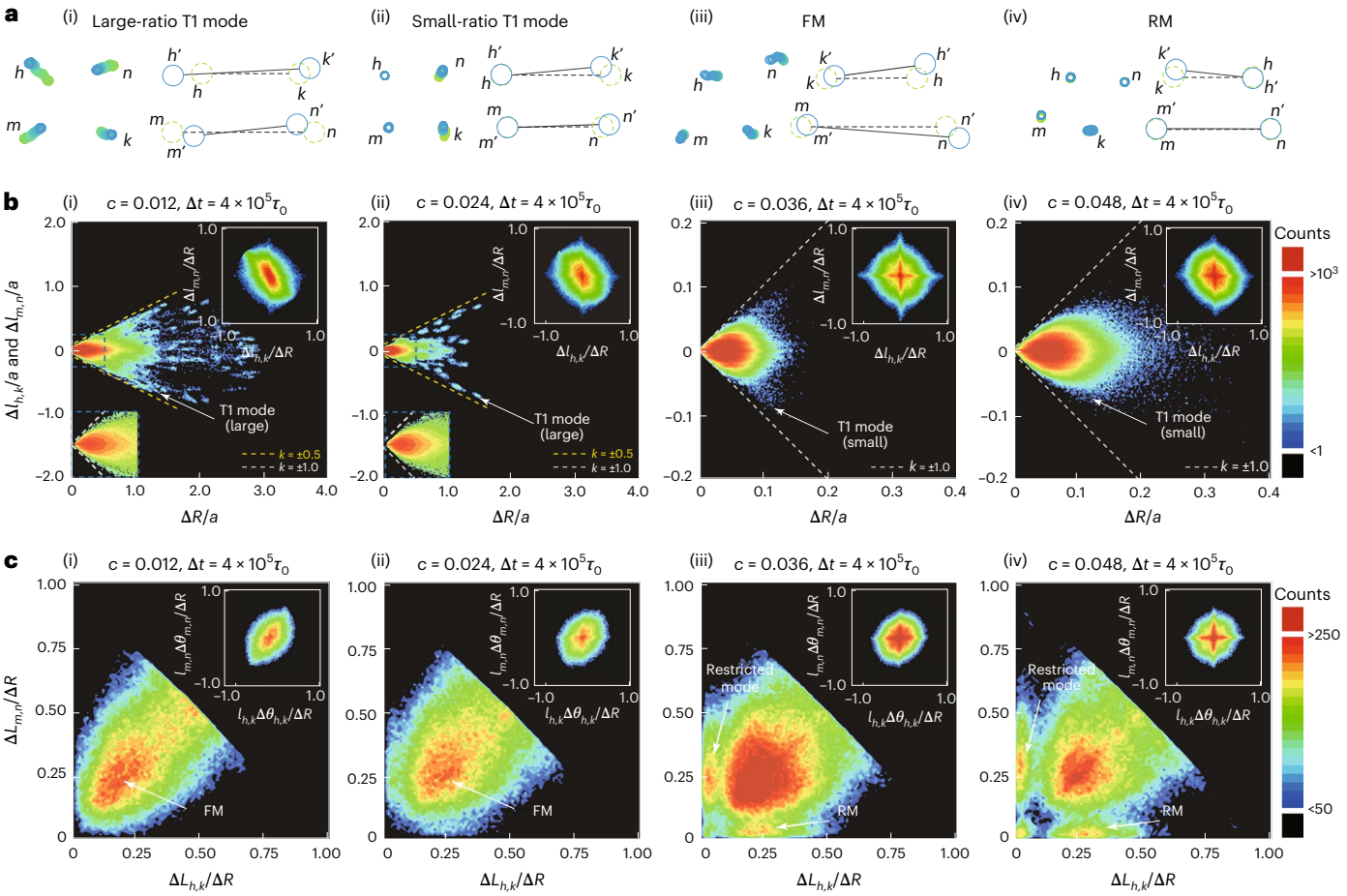

Fig. 3 | Four-particle tetragonal representation of the relaxation mode. **a**, Microscopic information of structural adjustment illustrated by a four-particle tetragon in fast-moving and slow-moving regions. From left to right: large-ratio T1 mode ($\Delta l_{h,k} \approx -\Delta l_{m,n}$), small-ratio T1 mode ($\Delta l_{h,k} \approx -\Delta l_{m,n}$), FM ($\Delta l_{h,k} \approx -\Delta l_{m,n}$ and $l_{h,k}\Delta\theta_{h,k} \approx l_{m,n}\Delta\theta_{m,n}$) and RM ($\Delta l_{h,k} \approx 0$, $\Delta\theta_{h,k} \approx 0$ or $\Delta l_{m,n} \approx 0$, $\Delta\theta_{m,n} \approx 0$). **b**, The $\{\Delta l_{h,k}, \Delta l_{m,n}\}$–$\Delta R$ counting map of the relaxation mode. From left to right: $c = 1.2\%$, $c = 2.4\%$, $c = 3.6\%$ and $c = 4.8\%$. The $\Delta l_{h,k}$–$\Delta l_{m,n}$ counting maps are shown in the insets. The orange dashed lines indicate $K = \pm 1/2$, whereas the white dashed lines indicate $K = \pm 1$. Evidently, the large-ΔR tetragon follows the T1 mode at $c \le c^*$, whereas the large-ratio T1 mode vanishes, and a signature of RM for small-ΔR tetragon emerges at $c > c^*$ (insets). Note that the x-axis range is different between the two left and two right panels. **c**, $\Delta L_{h,k}/\Delta R$–$\Delta L_{m,n}/\Delta R$ counting map of the relaxation mode. From left to right: $c = 1.2\%$, $c = 2.4\%$, $c = 3.6\%$ and $c = 4.8\%$. The $l_{h,k}\Delta\theta_{h,k}$–$l_{m,n}\Delta\theta_{m,n}$ counting maps are shown in the insets. The emergence of rigid bonds ($\Delta L_{h,k} \approx 0$ or $\Delta L_{m,n} \approx 0$) and development of RM at $c > c^*$ are evident.

Impact of interaction potential on local particle dynamics

Here we consider the effect of interaction range on the above scenario. In our system with long-range soft magnetic interactions, the slow dynamics in the form of small-ratio T1 events appears at $c \le c^*$ and persist at $c > c^*$, that is, $\tau_{\text{Small-T1}} \approx 10^5\tau_0$ at c^*, indicating that they belong to a slow β mode. To see what happens in systems with short-range interactions, we have performed experiments with 2D binary poly-*N*-isopropyl acrylamide (PNIPAM) colloidal systems (a model supercooled colloidal system with a short-range repulsive interaction; Methods). In this case, we find that the small-ratio T1 events are activated at the fast β regime ($\tau_{\text{Small-T1}} < \tau_0$), whereas clusters of large-ratio T1 events are slower and contribute to the string-like excitation (Extended Data Fig. 5a–f; note the red and orange strings of Δr formed in Extended Data Fig. 5f). Moreover, the string-like excitation can be reversible or directly serves as the precursors of α relaxation (Extended Data Fig. 5g–i; note the recovery of Δr at longer times (Extended Data Fig. 5g) for the orange string-like excitation in Extended Data Fig. 5f). These findings suggest that the slow activation process of small-ratio T1 events appears only deep in a glass state for systems with short-range interactions, which is consistent with the previous observation of sparse, localized defect excitations deep in a glass state[6,37]. Moreover, the typical MSD plateau value at the glass transition in our system with long-range interactions ($\langle \Delta r^2(t)/a^2 \rangle \approx 10^{-4}$) is 100 times smaller than the one in systems with hard, short-range interactions ($\langle \Delta r^2(t)/a^2 \rangle \approx 10^{-2}$) (refs. 6,37) (Extended Data Fig. 6a–c, left). Thus, interaction range and softness are critical parameters controlling whether the reversible bond-breaking process is fast or slow, that is, whether it belongs to fast or slow β modes, respectively. On the other hand, the string-like cage-breaking process universally serves as a precursor of α relaxation, irrespective of the interaction softness and range (Extended Data Fig. 5f–i).

We have noticed that besides the cage-breaking and bond-breaking processes, there is another type of structure change that does not accompany a topological change in the neighbour–neighbour connection network: passive displacement, that is, local elastic deformation, intrinsically coupled with T1 events. It remains elusive how this type of motion contributes to slow β and early α relaxations. To address this issue, we search for a possible relaxation mode linked to local deformation. To this end, we regard one neighbour–neighbour pair, $\{h, k\}$, as a two-particle 'bond', and decompose the bond motion, $\{\mathbf{r}_h(t + \Delta t) - \mathbf{r}_h(t), \mathbf{r}_k(t + \Delta t) - \mathbf{r}_k(t)\}$, where $\mathbf{r}_h$ and $\mathbf{r}_k$ are the position of particles h and k, respectively, into three parts: bond-length change $\Delta l_{h,k}$, bond reorientation $\Delta\theta_{h,k}$ and translational motion $\Delta p_{h,k}$ (Methods provides the definitions). Thus, the local deformation can be probed by these three elementary motions of the 'bonds'.

https://doi.org/10.1038/s41567-023-02016-4

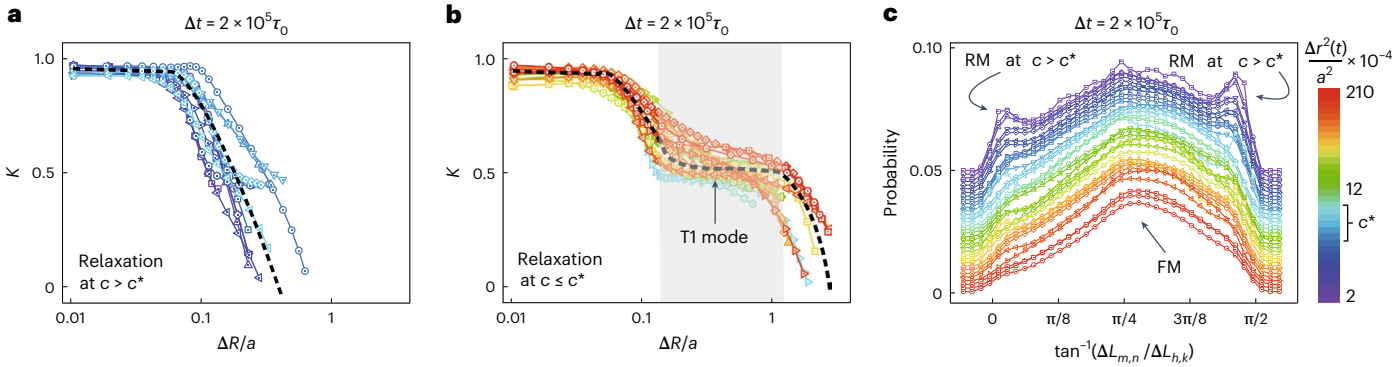

d

Class \ Types of motion	Large-ratio T1	Small-ratio T1	Other local motions
Type I, glass	None	Sparse, localized, slow β mode	FM, RM
Type I, liquid near T_g	String-like, precusor of α relaxation	Sparse, localized, slow β mode	FM, RM before large-ratio T1
Type II, liquid near T_g	String-like, slow reversible or precusor of α relaxation	Random, fast β mode	FM
Crystal	Slip of dislocation	None	Elastic mode

e

Class \ Coupling	Coupling and coexisting	Absent
Type I, glass	Small-ratio T1↓ RM↑	Large-ratio T1, α mode
Type I, liquid near T_g	Large-ratio T1 and small -ratio T1 coexist with FM	RM after large-ratio T1
Type II, liquid near T_g	Large-ratio T1 and small -ratio T1 coexist with FM	Slow small-ratio T1
Crystal	Large-ratio T1 coexists with elastic mode	Small-ratio T1, RM, slow β mode

Fig. 4 | Double signature of glass transition seen in internal relaxations. **a**,**b**, Change in K–ΔR master curve of all the samples with a reduction in internal relaxation. Evidently, the samples at $c \le c^*$ commonly have a $K \approx 1/2$ plateau ($0.3a \le \Delta R \le 1.2a$) for small-ratio and large-ratio T1 modes (**b**), where the relaxation follows the black dashed line. In contrast, samples at $c > c^*$ (**a**) follow another black dashed line without the $K \approx 1/2$ plateau for the large-ratio T1 mode. **c**, Probability distribution of FM and RM illustrated by the probability distribution of $\tan^{-1}(\Delta L_{m,n}/\Delta L_{h,k})$ for each sample. FM has a peak at around $\tan^{-1}(\Delta L_{m,n}/\Delta L_{h,k}) \approx \pi/4$ whereas RM has peaks at around $\tan^{-1}(\Delta L_{m,n}/\Delta L_{h,k}) \approx 0$ or $\tan^{-1}(\Delta L_{m,n}/\Delta L_{h,k}) \approx \pi/2$. Evidently, RM peaks emerge at around c^*, corresponding to the disappearance of the $K \approx 1/2$ plateau (**a**,**b**). **d**,**e**, Comparison of internal relaxation behaviours among amorphous systems with soft (Type I) and hard (Type II) interactions and crystalline systems.

For simplicity, we use the four-particle tetragon model $\{h, k, m, n\}$ (ref. 18) (Fig. 3 shows the T1 events). Here the two diagonal bonds $\{h, k\}$ and $\{m, n\}$ correspond to the nearest- and second-nearest-neighbour bonds, respectively.

Now, we study how the bond motion gives rise to tiny structure relaxation. We find two distinct relaxation modes characteristic of the slowly flowing and glass states of our system. In the slowly flowing samples ($c \le 3.0\%$) where large-ratio T1 events (the precursor of α relaxation) exist, a T1 tetragon is characterized by the relations $\Delta l_{h,k} \approx -\Delta l_{m,n}$ and $\Delta l_{h,k} \approx \frac{\Delta R}{2}$ (Figs. 3a(i)(ii) and 3b(i)(ii); here $\Delta R = \Sigma_{i=\{h,k,l,m\}}|\Delta \mathbf{r}(i)|$ is the total moving distance of the four particles), and a small-ΔR tetragon (slowly moving region) similar to $\Delta l_{h,k} \approx -\Delta l_{m,n}$ (Fig. 3a(iii) and Fig. 3b(i)(ii) (insets)). That is, one bond elongates whereas the other shrinks by a similar amount. In contrast, in the glass-state samples ($c > 3.0\%$) without large-ratio T1 events, a small-ΔR tetragon is characterized by another distinct signature: $\Delta l_{h,k} \approx 0$ or $\Delta l_{m,n} \approx 0$ (Fig. 3a(iv) or Fig. 3b(iii)(iv) (insets)), pointing to the restriction of bond deformation along specific directions. In this case, only one of the two bonds changes the length, and the other does not.

The bond reorientational motion $\Delta\theta$ also varies similar to Δl. In slowly flowing samples ($c \le 3.0\%$), we find that $l_{h,k}\Delta\theta_{h,k} \approx l_{m,n}\Delta\theta_{m,n}$ (Fig. 3c(i)(ii) (insets)). Thus, bonds $\{h, k\}$ and $\{m, n\}$ deform similar to the T1 event, which we identify as a flexible mode (FM) common to easy structure relaxation. In contrast, in the regime where a large-ratio T1 event is absent ($c > 3.0\%$), the relative motions, $\Delta\theta$ and Δl, are both depressed for one of the two diagonal bonds. Thus, the relative part of the bond motion in the glass-state samples is characterized by either

$$\Delta L_{h,k} \approx 0 \left(\Delta L_{h,k} = \sqrt{\Delta l_{h,k}^2 + (l_{h,k}\Delta\theta_{h,k})^2}\right)$$

or

$$\Delta L_{m,n} \approx 0 \left(\Delta L_{m,n} = \sqrt{\Delta l_{m,n}^2 + (l_{m,n}\Delta\theta_{m,n})^2}\right),$$

that is, no relative motion of one of the two bonds. These two relations can be confirmed by the emergence of two distinct patches close to the X and Y axes, respectively (Fig. 3c(iii)(iv); $\Delta t \approx 200\tau_s$). We note that the spontaneous fluctuation of a rigid patch is the first to occur within a timescale where the slow β mode is active, but the early α mode is not yet present—a sign that the system behaves as an 'experimental' glass that exhibits slow β relaxation (Extended Data Fig. 6a–c). Moreover, these 'rigid' bonds are spatially and temporally fluctuating in the system, and they are connected to form a percolated elastic network resisting the large-ratio T1 mode deep in a glass state (Extended Data Fig. 7)[38]. Structure relaxation, in this case, can be thought of as following a restricted mode (RM) under partial freezing of inside-cage motion. The enhancement in RM further decreases the frequency of reversible bond-breaking events (compare Extended Data Fig. 3 with Extended Data Fig. 7). Thus, as one goes deeper into the glassy state, the inside-cage motion is increasingly frozen, slowing down the slow β relaxation. In contrast to the system with long-range interactions, both RM and small-ratio T1-type slow β mode are absent in a supercooled liquid state for a system of short-range interactions and present only deep in a glass state (Extended Data Figs. 5a–i and 6a–c). This feature that these two modes appear and disappear together, hand in hand, suggests their inseparable relationship. Thus, we conclude that RM characterized by rigid bonds is a prerequisite for the emergence of the small-ratio T1-type slow β mode.

For large-ΔR tetragons, due to the dominance of the large-ratio T1 mode, their $\Delta l_{h,k}/\Delta R$ or $\Delta l_{m,n}/\Delta R$ should have an upper or lower bound of 1/2 or −1/2, respectively. In contrast, for low-ΔR tetragons, due to

the emergence of the RM mode in slowing-moving regions, $\Delta l_{h,k}/\Delta R$ or $\Delta l_{m,n}/\Delta R$ should have an upper or lower bound of 1 or −1 (Fig. 3b, dashed lines). Consequently, as ΔR reduces, the switching should occur from $K \approx 1/2$ (we define $K = \max(\Delta l_{h,k}/\Delta R)$) to $K \approx 1$ at a certain threshold value of $\Delta R^{\dagger}$. We can indeed see this switching in the K–ΔR master curve (Fig. 4a,b). Above $\Delta R^{\dagger}$, the cage-breaking dynamics at $c \le c^*$ is governed by the T1 mode; thus, we can observe a $K \approx 1/2$ plateau at $c \le c^*$ (Fig. 4b). Moreover, the disappearance of the $K \approx 1/2$ plateau coincides with the emergence of a distinct RM mode at $c > c^*$, which is evident in the probability distribution of FM and RM for all the samples (Fig. 4c). This transition behaviour suggests that the partial freezing of inside-cage motion and the disappearance of large-ratio T1 events are the double signatures that the system reaches a glass state with the slow β mode. This double signature at a particle level indicates an intrinsic connection between the initial α-relaxation stage and the faster internal β relaxation.

Discussion

The above finding can be intuitively explained as follows. The extra volume required for easy structure relaxations (free volume) is partially created by the inside-cage motion; thus, a string-like structure relaxation requires quasi-voids at the ends of a string[39] and the cooperation of inside-cage motion[30,39–43] that serves as a reservoir for facilitating free-volume transport. As the reservoir's capacity reduces, rigid bonds and the slow β mode emerge, the free-volume transport becomes difficult and a glass state is formed. This physical picture is consistent with the scenario that slow β relaxation is a type of restricted motion in regions of high glassiness of a supercooled liquid[11].

Here we stress that this double signature is absent for a crystalline state with dislocations. In our crystalline samples, we find that $\Delta l_{m,n}/\Delta l_{h,k} \approx \sqrt{3}$ (it should be an elastic mode); thus, there are no modes like FM and RM. More importantly, the relaxation of defective structures, that is, dislocations, belongs to large-ratio T1 events, and small-ratio T1 events are rarely seen in the system's relaxation. Therefore, the amorphous nature of the 'solid region' and the existence of extended or localized, complex 'soft spots' are the very origin of the unique small-amplitude relaxations and the resulting multistep structure relaxations, which are essentially different from its crystalline counterpart (Extended Data Figs. 5, 6 and 8 show a comparison of the modes in disordered and crystalline systems).

In our work, we consider the glassy dynamics in granular magnetic systems and colloidal suspensions, which serve as typical glass formers of soft and hard interactions. This allows us to classify glass formers into two limiting types, namely, Type I and Type II systems, according to the role of the subtle internal relaxation, that is, its contribution to the fast or slow β mode. First, we consider deeply supercooled liquids near the glass transition point T_g. For a Type I liquid, the slow activation of the small-ratio T1 events and the slower large-ratio T1 events can coexist, respectively, due to the small amplitude of inside-cage motion and the ease-of-flow characteristic of the potential softness. This is not the case for a Type II liquid due to the large amplitude of inside-cage motion. Thus, in a deeply supercooled state, the Type I liquid has a small-ratio T1-type slow β mode, whereas the Type II liquid has only a large-ratio-T1-type slow-subtle relaxation. This difference in the inside-cage motion also affects the dynamics in a glass state. For a glass state of the Type I system, we can always see the slow β mode, but it is not necessarily the case for the Type II system. For the Type II system, the small-ratio T1-type slow β mode should become evident only in a 'deep' glass state where the MSD plateau becomes so low that the large-ratio T1 events vanish and the small-ratio T1 events become dominant, slow and subtle relaxations. Thus, the critical factor separating Type I and Type II systems is the amplitude of the inside-cage motion, that is, the MSD plateau level, controlled by the potential softness. This scenario is supported by the microscopic information of internal relaxations observed in both amorphous and crystalline systems (Fig. 4d,e).

Concerning this classification, it is worth noting the recent finding of the difference in slow β relaxation between amorphous phase-change materials (PCMs) and non-PCM chalcogenide glasses[44,45], which showed that PCMs with softer bonds have much more pronounced slow β relaxations than non-PCMs with more rigid covalent bonds. Our scenario naturally explains this finding since more rigid restrictions on particle motion should make slow β relaxations weaker.

Our observations also suggest the universality of large-ratio T1 events serving as the precursors of α relaxation and the complexity of small-ratio T1 events that can be either fast or slow β relaxations, depending on the amplitude of inside-cage motion. Most glassy materials should lie between the two limits (Type I system with soft, long-range interactions and Type II system with hard, short-range interactions). It is an interesting question what happens in the intermediate-range interaction case.

Conclusion and outlook

In summary, we have experimentally found a qualitative change in the character of local structure adjustments of four neighbouring particles across a pinning-induced glass transition and revealed a non-trivial connection between structure relaxation modes that are intrinsic and unique to the glass system. We have shown that the emergence of bond rigidity kills string-like cage-breaking motion serving as a precursor of α relaxation. This emergence of rigid bonds accompanied by the freezing of structure relaxation can be regarded as a consequence of mechanical self-organization towards the emergence of solidity, that is, the percolation of force-bearing rigid bonds[38]. Increasing the pinning fraction, which should have a similar effect as lowering the temperature[26,27,32], should increase the bond rigidity[46], thus enhancing the glassy stability. In supercooled liquids, dynamic heterogeneity develops below the onset temperature of the super-Arrhenius behaviour. Slow α-relaxation regions with high glassy structural order[18,19,33,47–49], that is, low configurational entropy, can have transient rigidity characterized by the large Debye–Waller factor, that is, the small amplitude of inside-cage motion[50,51]. Considering that the small amplitude of inside-cage motion is necessary for activating small-ratio T1 events, this may explain the emergence of the slow β mode below the onset temperature and its spatial heterogeneity, which supports the argument made in another work[11].

Concerning the last point, another critical feature we find in a glass state is that particle motion in a glass state involves non-vibrational internal dynamics[4,5,52,53], that is, small-ratio T1 event and other cooperative bond-reorientation motion, besides vibrational motion. Previous studies suggested that many parameters, such as bond-orientational order[47], local packing capability[33,48], 'softness' parameter from machine learning[49] and parameter from local geometry[18,19], serve as good structure indicators of α relaxation. It implies that these indicators may also capture the information of tiny structure adjustments, that is, the bond reorientational motion, which may also be important in regions of slow structure relaxation in a supercooled liquid[11]. It looks natural to expect the link of high angular order[33,47,48] to the rigidity of bonds and the constraint on bond reorientation. It is interesting to see whether these structure indicators can predict the double signature, that is, the disappearance of cage breaking and the emergence of bond rigidity, for a glassy state. Their link to the Debye–Waller factor, that is, solidity, suggests such a possibility.

In this work, we focus on systems with isotropic interactions. The slow β relaxation of systems of anisotropic interactions, relevant for molecular systems, remains a critical issue for future research.

Online content

Any methods, additional references, Nature Portfolio reporting summaries, source data, extended data, supplementary information, acknowledgements, peer review information; details of author contributions and competing interests; and statements of data and code availability are available at https://doi.org/10.1038/s41567-023-02016-4.

References

1. Stevenson, J. D. & Wolynes, P. G. A universal origin for secondary relaxations in supercooled liquids and structural glasses. *Nat. Phys.* **6**, 62–68 (2010).
2. Zhang, Z., Ispas, S. & Kob, W. Roughness and scaling properties of oxide glass surfaces at the nanoscale. *Phys. Rev. Lett.* **126**, 066101 (2021).
3. Biroli, G. & Urbani, P. Breakdown of elasticity in amorphous solids. *Nat. Phys.* **12**, 1130–1133 (2016).
4. Ozawa, M., Ikeda, A., Miyazaki, K. & Kob, W. Ideal glass states are not purely vibrational: insight from randomly pinned glasses. *Phys. Rev. Lett.* **121**, 205501 (2018).
5. Yeh, W.-T., Ozawa, M., Miyazaki, K., Kawasaki, T. & Berthier, L. Glass stability changes the nature of yielding under oscillatory shear. *Phys. Rev. Lett.* **124**, 225502 (2020).
6. Scalliet, C., Berthier, L. & Zamponi, F. Nature of excitations and defects in structural glasses. *Nat. Commun.* **10**, 5102 (2019).
7. Saito, M. et al. Slow processes in supercooled *o*-terphenyl: relaxation and decoupling. *Phys. Rev. Lett.* **109**, 115705 (2012).
8. Ngai, K. L. & Paluch, M. Classification of secondary relaxation in glass-formers based on dynamic properties. *J. Chem. Phys.* **120**, 857–873 (2004).
9. Boyer, R. F. Dependence of mechanical properties on molecular motion in polymers. *Polym. Eng. Sci.* **8**, 161–185 (1968).
10. Johari, G. P. Glass transition and secondary relaxations in molecular liquids and crystals. *Ann. N. Y. Acad. Sci.* **279**, 117–140 (1976).
11. Tanaka, H. Origin of the excess wing and slow β relaxation of glass formers: a unified picture of local orientational fluctuations. *Phys. Rev. E* **69**, 021502 (2004).
12. Zuriaga, M. et al. New microscopic mechanism for secondary relaxation in glasses. *Phys. Rev. Lett.* **103**, 075701 (2009).
13. Zhao, Z. F., Wen, P., Shek, C. H. & Wang, W. H. Measurements of slow β-relaxations in metallic glasses and supercooled liquids. *Phys. Rev. B.* **75**, 174201 (2007).
14. Wang, Q. et al. Unusual fast secondary relaxation in metallic glass. *Nat. Commun.* **6**, 7876 (2015).
15. Yu, H.-B., Richert, R. & Samwer, K. Structural rearrangements governing Johari-Goldstein relaxations in metallic glasses. *Sci. Adv.* **3**, e1701577 (2017).
16. Zhang, H., Wang, X., Yu, H.-B. & Douglas, J. F. Dynamic heterogeneity, cooperative motion, and Johari–Goldstein β-relaxation in a metallic glass-forming material exhibiting a fragile-to-strong transition. *Eur. Phys. J. E* **44**, 56 (2021).
17. Franz, S., Parisi, G., Urbani, P. & Zamponi, F. Universal spectrum of normal modes in low-temperature glasses. *Proc. Natl Acad. Sci. USA* **112**, 14539–14544 (2015).
18. Bi, D., Lopez, J. H., Schwarz, J. M. & Manning, M. L. A density-independent rigidity transition in biological tissues. *Nat. Phys.* **11**, 1074–1079 (2015).
19. Bi, D., Yang, X., Marchetti, M. C. & Manning, M. L. Motility-driven glass and jamming transitions in biological tissues. *Phys. Rev. X* **6**, 021011 (2016).
20. Ngai, K. L. *Relaxation and Diffusion in Complex Systems* (Springer, 2011).
21. Scalliet, C., Guiselin, B. & Berthier, L. Excess wings and asymmetric relaxation spectra in a facilitated trap model. *J. Chem. Phys.* **155**, 064505 (2021).
22. Guiselin, B., Scalliet, C. & Berthier, L. Microscopic origin of excess wings in relaxation spectra of supercooled liquids. *Nat. Phys.* **18**, 468–472 (2022).
23. Dennis, R. C. & Corwin, E. I. Jamming energy landscape is hierarchical and ultrametric. *Phys. Rev. Lett.* **124**, 078002 (2020).
24. Charbonneau, P. et al. Numerical detection of the Gardner transition in a mean-field glass former. *Phys. Rev. E* **92**, 012316 (2015).
25. Berthier, L. et al. Growing timescales and lengthscales characterizing vibrations of amorphous solids. *Proc. Natl Acad. Sci. USA* **113**, 8397–8401 (2016).
26. Kob, W. & Berthier, L. Probing a liquid to glass transition in equilibrium. *Phys. Rev. Lett.* **110**, 245702 (2013).
27. Cammarota, C. & Biroli, G. Ideal glass transitions by random pinning. *Proc. Natl Acad. Sci. USA* **109**, 8850–8855 (2012).
28. Ozawa, M., Kob, W., Ikeda, A. & Miyazaki, K. Equilibrium phase diagram of a randomly pinned glass-former. *Proc. Natl Acad. Sci. USA* **112**, 6914–6919 (2015).
29. Cammarota, C. & Biroli, G. Aging and relaxation near random pinning glass transitions. *Europhys. Lett.* **98**, 16011 (2012).
30. Gokhale, S., Nagamanasa, K. H., Ganapathy, R. & Sood, A. K. Growing dynamical facilitation on approaching the random pinning colloidal glass transition. *Nat. Commun.* **5**, 4685 (2014).
31. Nagamanasa, K. H., Gokhale, S., Sood, A. K. & Ganapathy, R. Direct measurements of growing amorphous order and non-monotonic dynamic correlations in a colloidal glass-former. *Nat. Phys.* **11**, 403–408 (2015).
32. Angelani, L., Paoluzzi, M., Parisi, G. & Ruocco, G. Probing the non-Debye low-frequency excitations in glasses through random pinning. *Proc. Natl Acad. Sci. USA* **115**, 8700–8704 (2018).
33. Tong, H. & Tanaka, H. Revealing hidden structural order controlling both fast and slow glassy dynamics in supercooled liquids. *Phys. Rev. X* **8**, 011041 (2018).
34. Li, B., Lou, K., Kob, W. & Granick, S. Anatomy of cage formation in a two-dimensional glass-forming liquid. *Nature* **587**, 225–229 (2020).
35. Watanabe, K., Kawasaki, T. & Tanaka, H. Structural origin of enhanced slow dynamics near a wall in glass-forming systems. *Nat. Mater.* **10**, 512–520 (2011).
36. Stevenson, J. D., Schmalian, J. & Wolynes, P. G. The shapes of cooperatively rearranging regions in glass-forming liquids. *Nat. Phys.* **2**, 268–274 (2006).
37. Scalliet, C., Berthier, L. & Zamponi, F. Absence of marginal stability in a structural glass. *Phys. Rev. Lett.* **119**, 205501 (2017).
38. Tong, H., Sengupta, S. & Tanaka, H. Emergent solidity of amorphous materials as a consequence of mechanical self-organisation. *Nat. Commun.* **11**, 4863 (2020).
39. Yip, C.-T. et al. Direct evidence of void-induced structural relaxations in colloidal glass formers. *Phys. Rev. Lett.* **125**, 258001 (2020).
40. Chandler, D. & Garrahan, J. P. Dynamics on the way to forming glass: bubbles in space-time. *Annu. Rev. Phys. Chem.* **61**, 191–217 (2010).
41. Vogel, M. & Glotzer, S. C. Spatially heterogeneous dynamics and dynamic facilitation in a model of viscous silica. *Phys. Rev. Lett.* **92**, 255901 (2004).
42. Keys, A. S., Hedges, L. O., Garrahan, J. P., Glotzer, S. C. & Chandler, D. Excitations are localized and relaxation is hierarchical in glass-forming liquids. *Phys. Rev. X* **1**, 021013 (2011).
43. Mishra, C. K., Nagamanasa, K. H., Ganapathy, R., Sood, A. K. & Gokhale, S. Dynamical facilitation governs glassy dynamics in suspensions of colloidal ellipsoids. *Proc. Natl Acad. Sci. USA* **111**, 15362–15367 (2014).
44. Cheng, Y. et al. Highly tunable β-relaxation enables the tailoring of crystallization in phase-change materials. *Nat. Commun.* **13**, 7352 (2022).
45. Peng, S.-X. et al. Uncovering β-relaxations in amorphous phase-change materials. *Sci. Adv.* **6**, eaay6726 (2020).

46. Ji, W., de Geus, T. W. J., Popović, M., Agoritsas, E. & Wyart, M. Thermal origin of quasilocalized excitations in glasses. *Phys. Rev. E* **102**, 062110 (2020).
47. Tanaka, H. Bond orientational order in liquids: towards a unified description of water-like anomalies, liquid-liquid transition, glass transition, and crystallization. *Eur. Phys. J. E* **35**, 113 (2012).
48. Tong, H. & Tanaka, H. Structural order as a genuine control parameter of dynamics in simple glass formers. *Nat. Commun.* **10**, 5596 (2019).
49. Cubuk, E. D. et al. Structure-property relationships from universal signatures of plasticity in disordered solids. *Science* **358**, 1033–1037 (2017).
50. Widmer-Cooper, A. & Harrowell, P. Predicting the long-time dynamic heterogeneity in a supercooled liquid on the basis of short-time heterogeneities. *Phys. Rev. Lett.* **96**, 185701 (2006).
51. Kawasaki, T., Araki, T. & Tanaka, H. Correlation between dynamic heterogeneity and medium-range order in two-dimensional glass-forming liquids. *Phys. Rev. Lett.* **99**, 215701 (2007).
52. Scalliet, C. & Berthier, L. Rejuvenation and memory effects in a structural glass. *Phys. Rev. Lett.* **122**, 255502 (2019).
53. Albert, S. et al. Fifth-order susceptibility unveils growth of thermodynamic amorphous order in glass-formers. *Science* **352**, 1308–1311 (2016).

Methods

Experiments with magnetic discs

Particulate glassy systems that enable single-particle-level dynamic observation, such as colloids[39,54,55], granular systems and emulsions[5,56,57], have provided valuable particle-level information on various types of glassy dynamics, including dynamic heterogeneity in a supercooled liquid[31,54], micromechanical responses of glasses under shear or non-equilibrium excitations[5,34,56], Gardner-like dynamics[56,58] and quasi-localized vibrational modes[57,59]. Various experimental techniques, such as particle pinning[30,31] and the introduction of activity and other non-equilibrium excitations[34,60], have also been employed to control glass transition. However, combining a high spatial resolution with an ultralong-time observation has been challenging in colloidal systems because of many technical problems, such as gradual solvent evaporation and a slight colloid–solvent density mismatch that cause the density change or flow of the sample. A mechanical-driven granular system is suitable for long-time single-particle-level observation because it is free from these problems. However, for hard-sphere particles, the particle–particle contact friction brings complexity to the glassy dynamics. We use granular particles interacting with long-range repulsion to realize a system free from interparticle contact friction.

To this end, we use a unique experimental setup (Fig. 1a), in which a 2D binary magnetic-disc mixture confined in an upper sample cell is mechanically perturbed by the motion of the bottom plate through long-range magnetic interactions. We fix the perturbation strength so that the system is slightly above the glass transition point. Then, under this perturbation, we change the fraction of pinned particles to control the effective temperature of the system. This specially designed system allows us to precisely measure local structural rearrangements over an extremely long time, covering from slightly above to far below the pinning-induced glass transition.

To probe structure relaxations in a crystalline system with dislocations, we use large magnetic discs (10 mm diameter) employed in our glass system. Then, we form a 2D hexagonal crystalline structure with dislocations (Extended Data Fig. 5g,h). We adjust the perturbation strength to a value such that the MSD plateau value is around 4×10^{-4} (Extended Data Fig. 6d).

Experiments with colloidal particles

The 2D monolayer colloidal sample is prepared by loading a 1:1 binary mixture of PNIPAM particles (1.0 and 1.3 μm at 22 °C) between two coverslips. The samples are then hermetically sealed using optical glue (Norland 63). The interactions between PNIPAM particles can be characterized as short-range hard-core repulsions[59]. The sample has a packing fraction of 0.88 at ambient temperature and is continuously imaged with standard bright-field microscopy at the rate of 20 frames per second for a duration of 40,000 frames. The trajectory of each particle is extracted by particle-tracking techniques. Note that the colloidal sample is not suitable for ultralong-time single-particle-level observation.

Structure and dynamic analyses

The global relaxation dynamics is characterized by the MSD of all the particles, $\langle \Delta \mathbf{r}^2(t) \rangle = \frac{1}{N} \sum_{j=1}^{N} \langle [\mathbf{r_i}(t) - \mathbf{r_i}(0)]^2 \rangle$, where N is the number of particles and $\mathbf{r_i}(t) - \mathbf{r_i}(0)$ is the displacement, $\Delta \mathbf{r}(i)$, during a lag time t for particle i.

We use the self-part of a particle-level Van Hove function G_{si} to quantify the dynamics of the fastest mobile particles: $G_{\mathrm{si}}(r,t) = \frac{1}{N_f} \sum_{i=1}^{N_f} \langle \delta(\mathbf{r} - |\mathbf{r_i}(t) - \mathbf{r_i}(\mathbf{0})|) \rangle$, where δ is the delta function and N_f is the number of particles that have a narrow range of $\langle \Delta \mathbf{r}_i^2(t) \rangle (\Delta t = 500\tau_s)$. It efficiently probes the 'caged-then-jumping' dynamics at specific distances. Purely vibrational motion exhibits a Gaussian distribution in this function, whereas the 'caged-then-jumping' motion should form a second peak or shoulder at a characteristic moving distance.

Relaxation-mode analysis

We define the neighbours of particle i at each time t through the Voronoi tessellation. For particle i, the neighbour-change parameter $N_b(i)$ is defined as the number of neighbours that are lost and gained after Δt.

We use the four-particle tetragon model to quantify the structural adjustment modes. Four neighbouring particles, $\{h, k, m, n\}$, form a tetragon. The tetragon has two diagonal bonds. We identify the bond $\{h, k\}$ as the nearest-neighbour diagonal bond and $\{m, n\}$ as the second-nearest one at the initial time. We define the total moving distance ΔR for each tetragon during a lag time Δt as $\Delta R = \Sigma_{i=\{h,k,l,m\}} |\Delta \mathbf{r_i}(\Delta t)|$. On the T1 event, $\{h, k, m, n\}$ experience a topological change, by which the two diagonal bonds $\{h, k\}$ and $\{m, n\}$ become the second-nearest and nearest diagonal bonds, respectively. We characterize the amplitude of a T1 event by l_{sl}, which is the time average of the normalized difference between the long diagonal length l_{long} and short diagonal length l_{short} of the T1 tetragon, namely, $l_{\mathrm{sl}} = \langle (l_{\mathrm{long}} - l_{\mathrm{short}})/l_{\mathrm{long}} \rangle$ (note that particle i may have two values of $l_{\mathrm{sl}}(i)$ if it is involved in two different T1 events).

For each bond $\{h, k\}$, we decompose the bond motion as $\{\mathbf{r_h}(t + \Delta t) - \mathbf{r_h}(t), \mathbf{r_k}(t + \Delta t) - \mathbf{r_k}(t)\}$, where $\mathbf{r_h}$ and $\mathbf{r_k}$ are the position of particle h and particle k, respectively, into three parts: bond-length change $\Delta l_{h,k}$, bond reorientation $\Delta \theta_{h,k}$ and translational motion $\Delta p_{h,k}$. Here $\Delta l_{h,k} = |\mathbf{r_h}(t + \Delta t) - \mathbf{r_k}(t + \Delta t)| - |\mathbf{r_h}(t) - \mathbf{r_k}(t)|$; $\Delta \theta_{h,k} = \theta(t + \Delta t) - \theta(t)$, where θ is the angle of vector $\mathbf{r_h} - \mathbf{r_k}$ with respect to the x axis; and $\Delta p_{h,k} = \frac{(|\mathbf{r_h}(t+\Delta t) + \mathbf{r_k}(t+\Delta t) - \mathbf{r_h}(t) - \mathbf{r_k}(t)|)}{2}$. For simplicity, we define the relative part of bond motion $\Delta L_{h,k}$ as $\Delta L_{h,k} = \sqrt{\Delta l_{h,k}^2 + (l_{h,k} \Delta \theta_{h,k})^2}$, where $l_{h,k}$ is the time-averaged bond length.

The emergence of the rigid bond is characteristic of spatiotemporal fluctuations of a glass state. Within our observation time of $10^3 \tau_s$, we can choose a time interval Δt as $\Delta t \approx 200\tau_s$, and use the $\Delta L_{h,k}/\Delta R - \Delta L_{m,n}/\Delta R$ counting map (Fig. 3c) to pick up the bonds in a 'rigid' state, which are spatially and temporally fluctuating in the system. Thus, for a specific bond, we can define its rigidity through the time over which its dynamics belong to RM and not FM. We define a bond with more than 15% of its time fluctuating on a 'rigid' state as a 'rigid' bond (Extended Data Fig. 5 shows their spatiotemporal fluctuations).

String-like excitation

Particles with $\Delta r \geq 0.3a$ are regarded as undergoing cage-breaking motion. Additionally, cage-breaking particles with their displacement vectors $\mathbf{r_i}(t) - \mathbf{r_i}(0)$ pointing to their neighbouring particles at $t = 0$ are defined as string-like excitation. We can see this feature (Fig. 2e,f, red and orange arrows) for large-ratio T1 events.

Data availability

The data that support the findings of this study are available from the corresponding authors upon reasonable request.

Code availability

The codes used in this study are available from the corresponding authors upon reasonable request.

References

54. Weeks, E. R., Crocker, J. C., Levitt, A. C., Schofield, A. & Weitz, D. A. Three-dimensional direct imaging of structural relaxation near the colloidal glass transition. *Science* **287**, 627–631 (2000).
55. Zheng, Z., Wang, F. & Han, Y. et al. Glass transitions in quasi-two-dimensional suspensions of colloidal ellipsoids. *Phys. Rev. Lett.* **107**, 065702 (2011).
56. Scalliet, C., Gnoli, A., Puglisi, A. & Vulpiani, A. Cages and anomalous diffusion in vibrated dense granular media. *Phys. Rev. Lett.* **114**, 198001 (2015).
57. Lin, J., Jorjadze, I., Pontani, L.-L., Wyart, M. & Brujic, J. Evidence for marginal stability in emulsions. *Phys. Rev. Lett.* **117**, 208001 (2016).

58. Hammond, A. P. & Corwin, E. I. Experimental observation of the marginal glass phase in a colloidal glass. *Proc. Natl Acad. Sci. USA* **117**, 5714–5718 (2020).
59. Chen, K. et al. Measurement of correlations between low-frequency vibrational modes and particle rearrangements in quasi-two-dimensional colloidal glasses. *Phys. Rev. Lett.* **107**, 108301 (2011).
60. Lozano, C., Gomez-Solano, J. R. & Bechinger, C. Active particles sense micromechanical properties of glasses. *Nat. Mater.* **18**, 1118–1123 (2019).

Acknowledgements

P.T. acknowledges the National Natural Science Foundation of China (nos. 12174071, 12105050, 12035004, 11734014 and 11725521), the Innovation Program of Shanghai Municipal Education Commission (no. 2023ZKZD06) and the Science and Technology Commission of Shanghai Municipality (no. 20JC1414700). Y.C. acknowledges the China Postdoc Science Foundation (nos. BX2021081 and 2021M690707). H. Tanaka acknowledges the Grants-in-Aid for Specially Promoted Research (JP20H05619) from the Japan Society for the Promotion of Science (JSPS).

Author contributions

P.T. and H. Tanaka conceived and supervised the research, performed the data analysis and modelling, and wrote the paper. Y.C. performed the experiments, data analysis and modelling. Z.Y. performed the experiments and data analysis. K.W. and J.H. performed the data analysis. H. Tong and Y.J. performed the data analysis and modelling, and K.C. performed the colloidal experiments.

Competing interests

The authors declare no competing interests.

Additional information

Extended data is available for this paper at https://doi.org/10.1038/s41567-023-02016-4.

Supplementary information The online version contains supplementary material available at https://doi.org/10.1038/s41567-023-02016-4.

Correspondence and requests for materials should be addressed to Hajime Tanaka or Peng Tan.

Peer review information *Nature Physics* thanks Jana Shanelova and Shuai Wei for their contribution to the peer review of this work.

https://doi.org/10.1038/s41567-023-02016-4

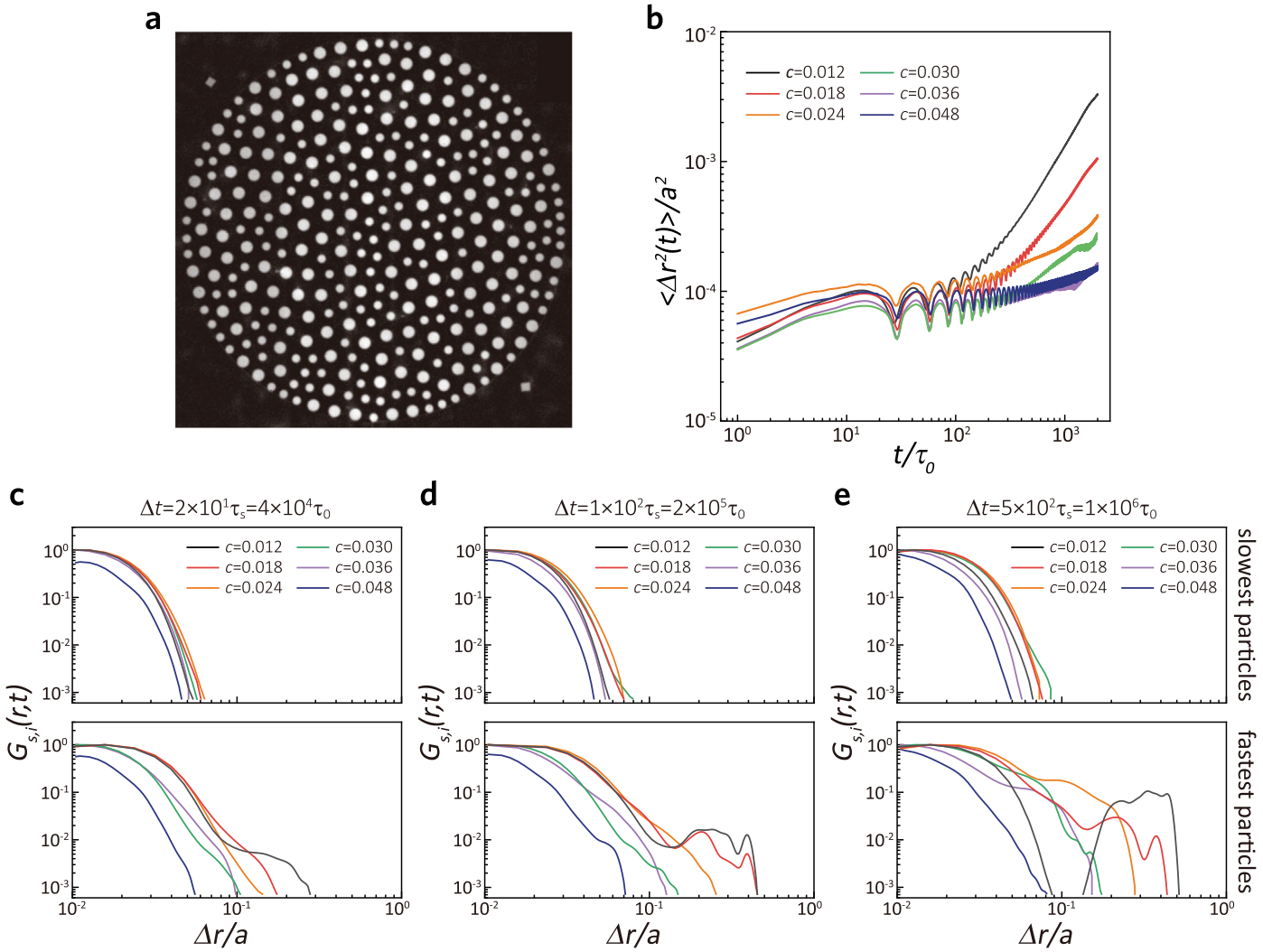

Extended Data Fig. 1 | Our 2D binary magnetic disk system under mechanical perturbation. a, A typical raw image of our sample. **b**, MSD of our pinning samples over τ_s at a high perturbation strength. Within τ_s, we can see a significant rise from the MSD plateau, which means that the system behaves as a viscous fluid. In this case, the long-time MSD becomes superdiffusive under our mechanical perturbation. With increasing the pinning fraction c, we can see that the system's response gradually becomes solid-like. Thus, the mechanical perturbation strength should be small enough to guarantee a solid-like response within τ_s. **c-e**, Relaxation dynamics illustrated by the particle-level Van Hove correlation function at $\Delta t = 20\tau_s$(**c**), $\Delta t = 100\tau_s$ (**d**), and $\Delta t = 500\tau_s$ (**e**). The self part of the particle-level time-dependent Van Hove correlation function, $G_{s,i}(r, t)$, is calculated for a group of particles i that have a narrow range of $\langle \Delta r^2(t) \rangle$ ($\Delta t = 500\tau_s$). The long-time motion of the fastest particles forms a second peak or a shoulder at a characteristic moving distance, whereas the motion of the slowest particles exhibits a Gaussian distribution.

https://doi.org/10.1038/s41567-023-02016-4

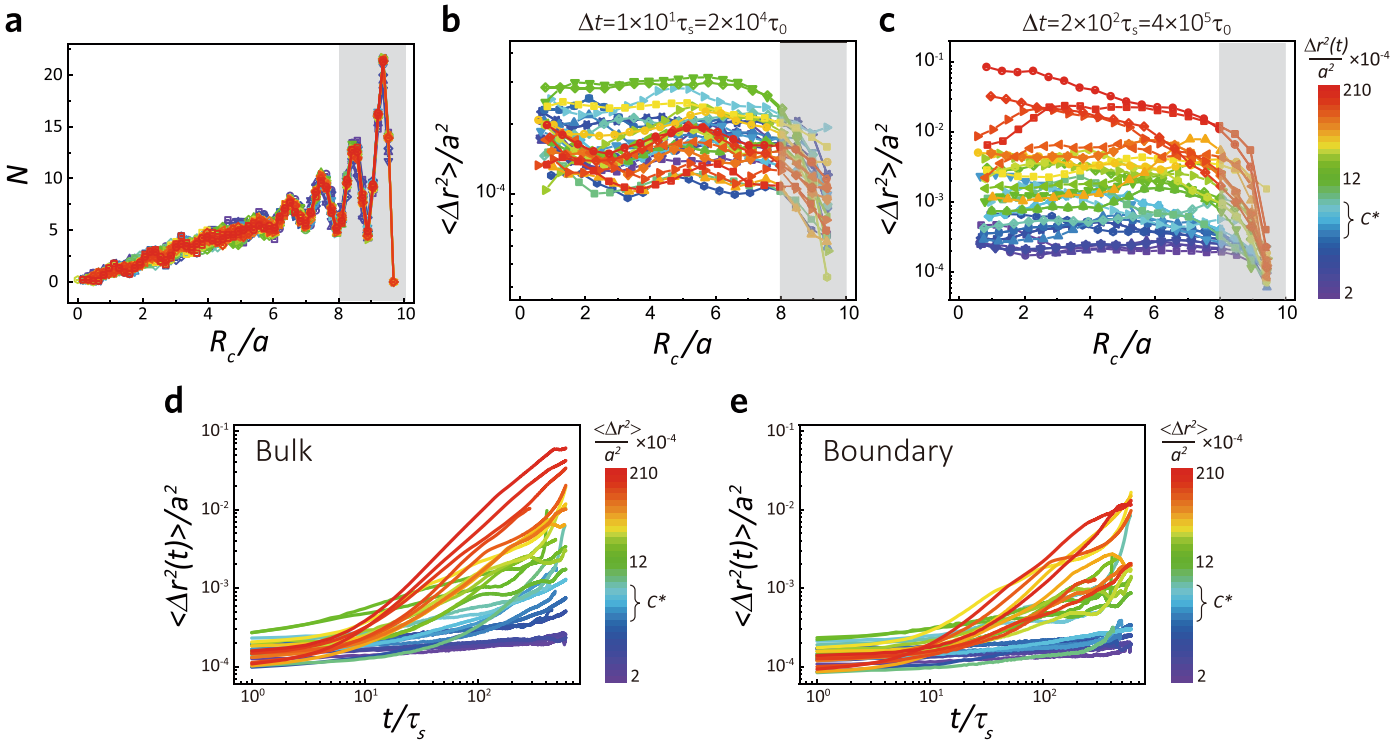

Extended Data Fig. 2 | Wall-induced effects on the relaxation dynamics in our systems. a, The particle number N counted with respect to the distance R_C/a from the centre. The smooth circular wall induces the layering of particles up to a distance around $2a$ (a grey area) from the wall. **b, c**, Particles' mean-square displacements (MSD), $\langle\Delta r^2(t)\rangle/a^2$, with respect to R_C/a at $\Delta t = 10\tau_s$ (**b**) and $\Delta t = 200\tau_s$ (**c**). The wall slows down the particle motion near the wall (a grey area). **d, e**, $\langle\Delta r^2(t)\rangle/a^2$ of bulk particles (**d**) and boundary particles (**e**). Although particles near the wall have slower dynamics than the bulk particles, we can observe the same threshold value of c^*. It indicates that the wall does not change the glass transition point but makes the system less fragile, that is, stronger.

https://doi.org/10.1038/s41567-023-02016-4

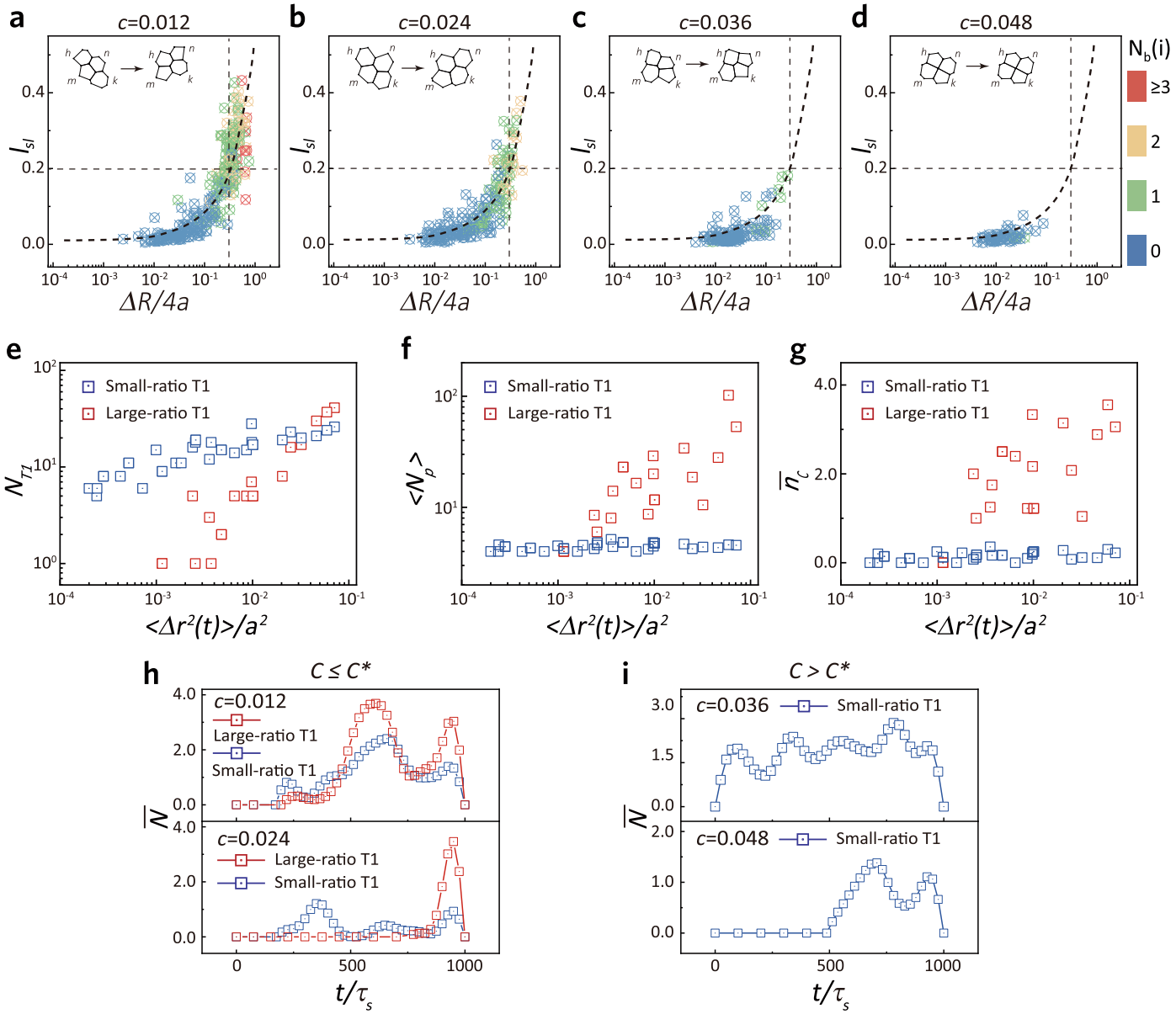

Extended Data Fig. 3 | Characterization of internal-relaxation profiles. **a-d**, The unified $l_{s,l} - \Delta R$ relation for T1 events. **a**, c ~ 0.012, **b**, c ~ 0.024, **c**, c ~ 0.036, **d**, c ~ 0.048. Here, ΔR is the total moving distance of the four particles in each tetragon. We can see a similar curve as in Fig. 2a-d. Note that each tetragon has four values of $N_b(i)$. **e-g**, Cluster analysis of large-T1 and small-T1 events for all samples as a function of $\langle \Delta r^2(t = 200\tau_s)\rangle/a^2$, where c^* is located around $\langle \Delta r^2(t)\rangle/a^2 \sim 10^{-3}$. **e**, The number of T1-tetragon, N_{T1}, in each sample. **f**, The average particle number, $\langle N_P\rangle$, contained in the T1-cluster. **g**, The coordination number, $\overline{n_c}$, of T1-tetragon in the T1 cluster. Large-T1 cluster is string-like cooperative excitation at $c \le c^*$ ($\langle N_P\rangle \sim 10$, $\overline{n_c} \sim 2$), whereas small-T1 cluster is sparse, localized excitation at all c ($\langle N_P\rangle \sim 4$, $\overline{n_c} \sim 0$). **h, i**, The number of T1-tetragon, $\overline{N}$, excited with respect to t at $c < c^*$ (**h**) and $c > c^*$ (**i**). Large-T1 and small-T1 events are excited at different time scales, suggesting that small-T1 event contributes to slow-β relaxation.

https://doi.org/10.1038/s41567-023-02016-4

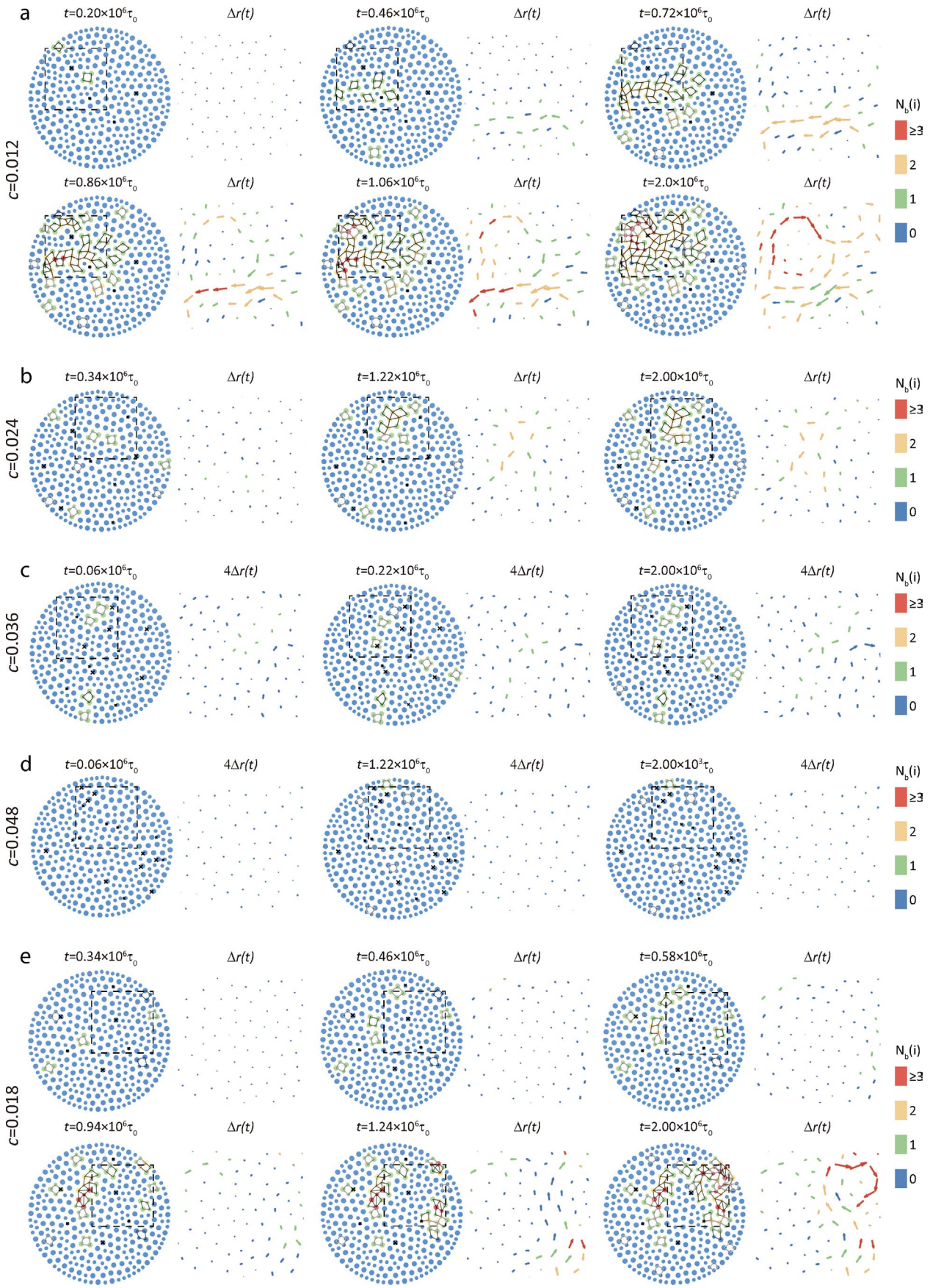

Extended Data Fig. 4 | See next page for caption.

https://doi.org/10.1038/s41567-023-02016-4

Extended Data Fig. 4 | Spatio-temporal illustration of internal-relaxation dynamics with increasing the pinning fraction. Relaxation dynamics is illustrated by $\Delta R(i)$ (indicated by the arrow length and direction), l_{s1} (indicated by black and grey tetragons representing large-ratio and small-ratio T1 events, respectively), and $N_b(i)$ (indicated by the particle and displacement colours). **a**, Sequential accumulation of large-ratio T1 events forms a compact cluster with $N_b(i)\geq 1$ for a typical sample of α-type relaxation ($c \sim 1.2\%$). Note that the motion that forms the cluster's core is also string-like. **b**, A collective excitation of spatially extended large-ratio T1 events forms a string-like cage-breaking excitation for a typical sample at $c \sim 2.4\%$. **c** and **d** correspond to the cases of a glass state ($c \sim 3.6\%$ and $c \sim 4.8\%$ respectively), where large-ratio T1 events vanishes, but localized small-ratio T1 events can persist. The displacement fields in **c** and **d** are magnified 4 times. **e**, Sequential accumulation of large-T1 events that develop into a string-like larger cluster at a pinning fraction similar to **a**.

https://doi.org/10.1038/s41567-023-02016-4

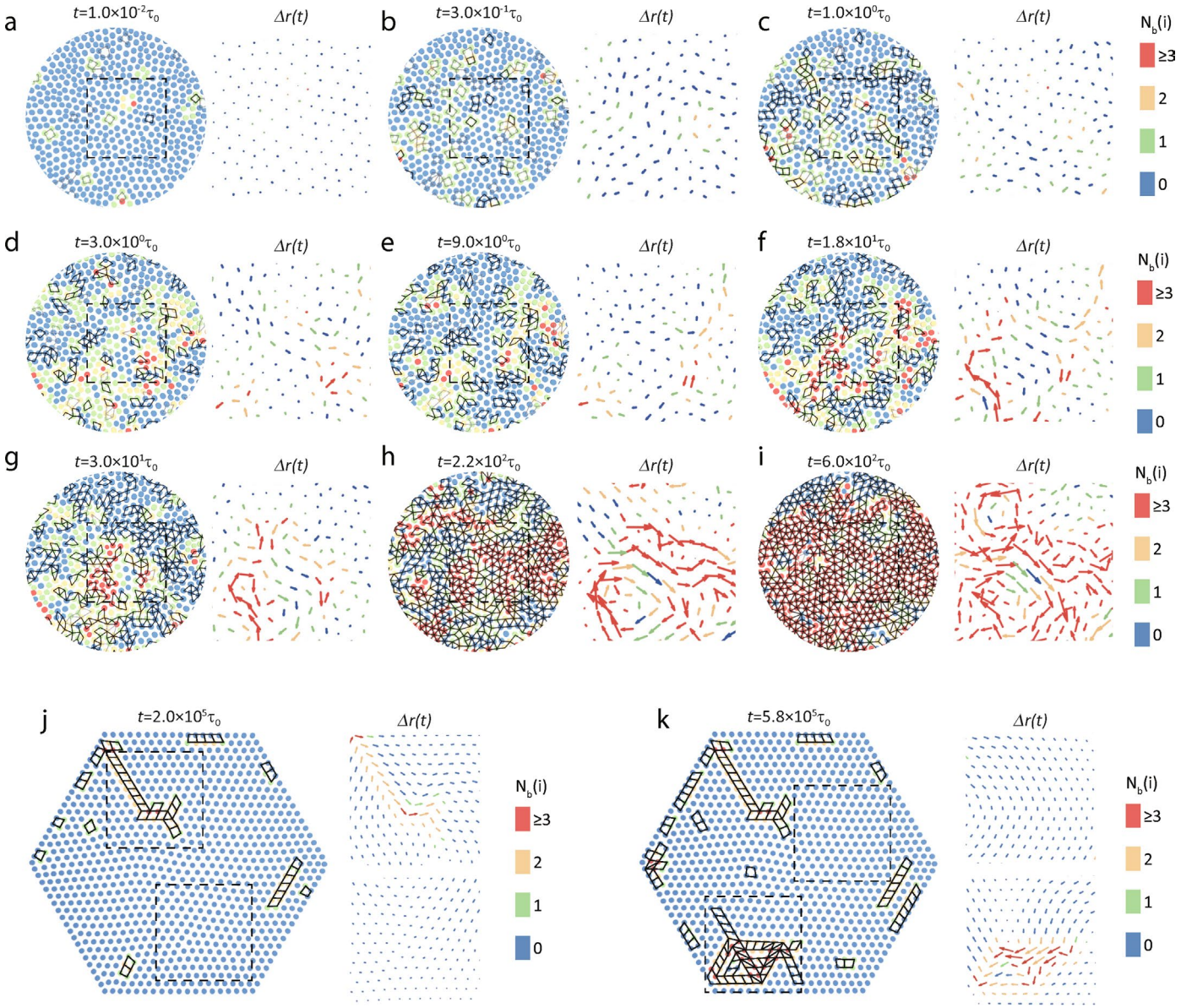

Extended Data Fig. 5 | Spatio-temporal illustration of internal-relaxation dynamics in a supercooled colloidal liquid and a granular, crystalline system with dislocations. We use bidisperse Nipam colloidal particles to form a 2D glassy system. Relaxation dynamics is illustrated by $\Delta r(i)$ (indicated by the arrow length and direction), l_{sl} (indicated by black and grey tetragons representing large-ratio and small-ratio T1 events, respectively), and $N_b(i)$ (indicated by the particle and the displacement colours). **a-c**, Reversible bond-breaking process occurring at the fast-β regime ($t < \tau_0$). **d-f**, Formation of string-like excitation after the fast-β regime. See the red and orange strings of Δr in **f**. **g-i**, Irreversible cage-breaking events serving as precursors of relaxation. See the recovery of Δr in **g** for the orange string in **f**. **j, k**, Spatial illustration of structure relaxations in a crystalline system with dislocations. We use large disk particles (10 mm diameter) in our magnetic glass system to form the 2D hexagonal crystalline structure with dislocations. Dislocation dynamics is responsible for large-ratio T1 events. We rarely find small-ratio T1 events, indicating the absence of the slow-β mode.

https://doi.org/10.1038/s41567-023-02016-4

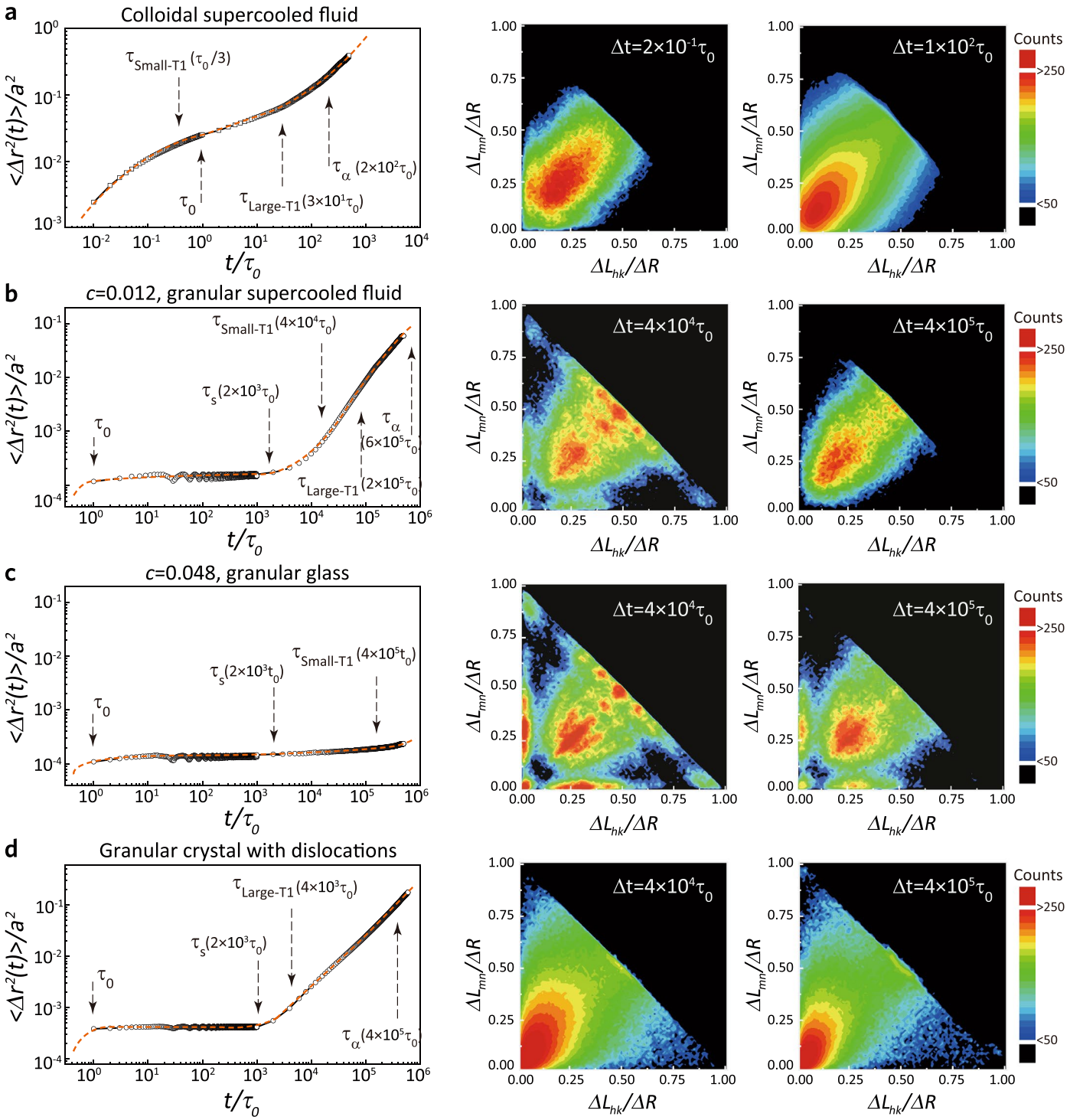

Extended Data Fig. 6 | Comparison of the relaxation dynamics for two glass systems and crystals, using the four-particle tetragon model. a, A colloidal supercooled colloidal liquid system with short-range interactions that represents fast-β and α modes. We use bidisperse Nipam colloidal particles to form 2D glassy system. Note that the MSD plateau value is around 2.0×10^{-2}. Small-ratio T1 events occur within τ_0, whereas large-ratio T1 events typically occur around a time of 30 τ_0 (left panel). RM is absent for the relaxation dynamics examined at $\Delta t = 0.2\tau_0$ (middle panel) and $\Delta t = 100\tau_0$ (right panel). **b**, The deeply supercooled granular liquid sample with long-range soft interaction that represents slow-β and α modes (c ~ 1.2%). Note that the MSD plateau value is around 2.0×10^{-4}. Small-ratio T1 events typically occur around a time of $2.0\times10^4\tau_0$, whereas large-ratio T1 events typically occur around a time of $1.0\times10^5\tau_0$ (left panel). We find a weak signature of RM at the time scale of slow-β relaxation (middle panel), whereas RM is absent at the timescale of early-α relaxation (right panel). **c**, The granular glass sample with long-range soft interaction that represents slow-β mode (c = 4.8%). Note that the MSD plateau value is around 4.0×10^{-4}. Small-ratio T1 events typically occur around a time of $2.0\times10^5\tau_0$, whereas large-ratio T1 events are absent (left panel). We find a strong signature of RM at the time scale shorter than (middle panel) and comparable (right panel) to the slow-β relaxation time. **d**, The crystalline system with dislocations. We use large disk particles (10 mm diameter) used in our glass system to form a 2D hexagonal crystalline structure with dislocations. Both RM and small-T1 events are absent.

https://doi.org/10.1038/s41567-023-02016-4

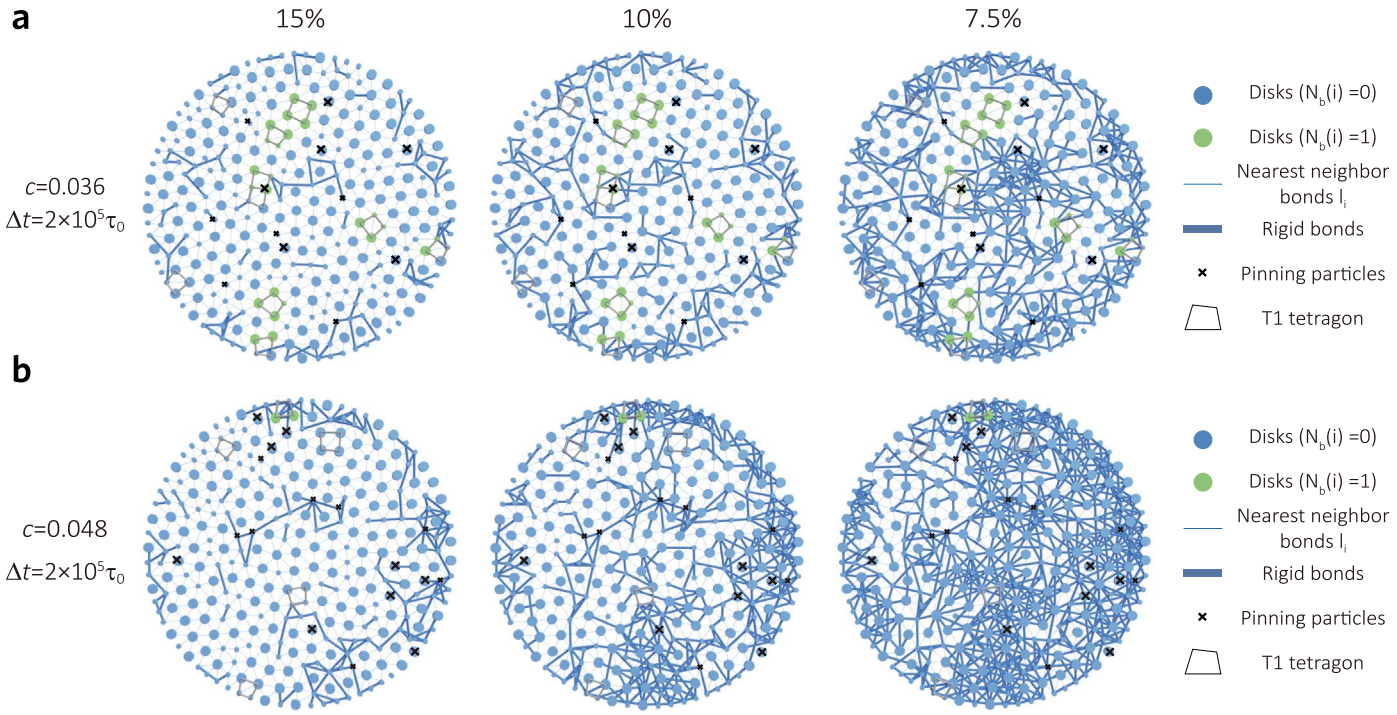

Extended Data Fig. 7 | Spontaneous fluctuations of 'rigid' bonds in glass samples. a, c ~ 3.6%, **b**, c ~ 4.8%. For a specific bond, we can define its rigidity through the time percentage that its dynamics belongs to the RM mode and not to the FM mode. The bonds with more than 7.5%, 10%, and 15% of their time in a 'rigid' state are shown. We can see spontaneous fluctuations of 'rigid' bonds that present RM when approaching a glass state.

https://doi.org/10.1038/s41567-023-02016-4

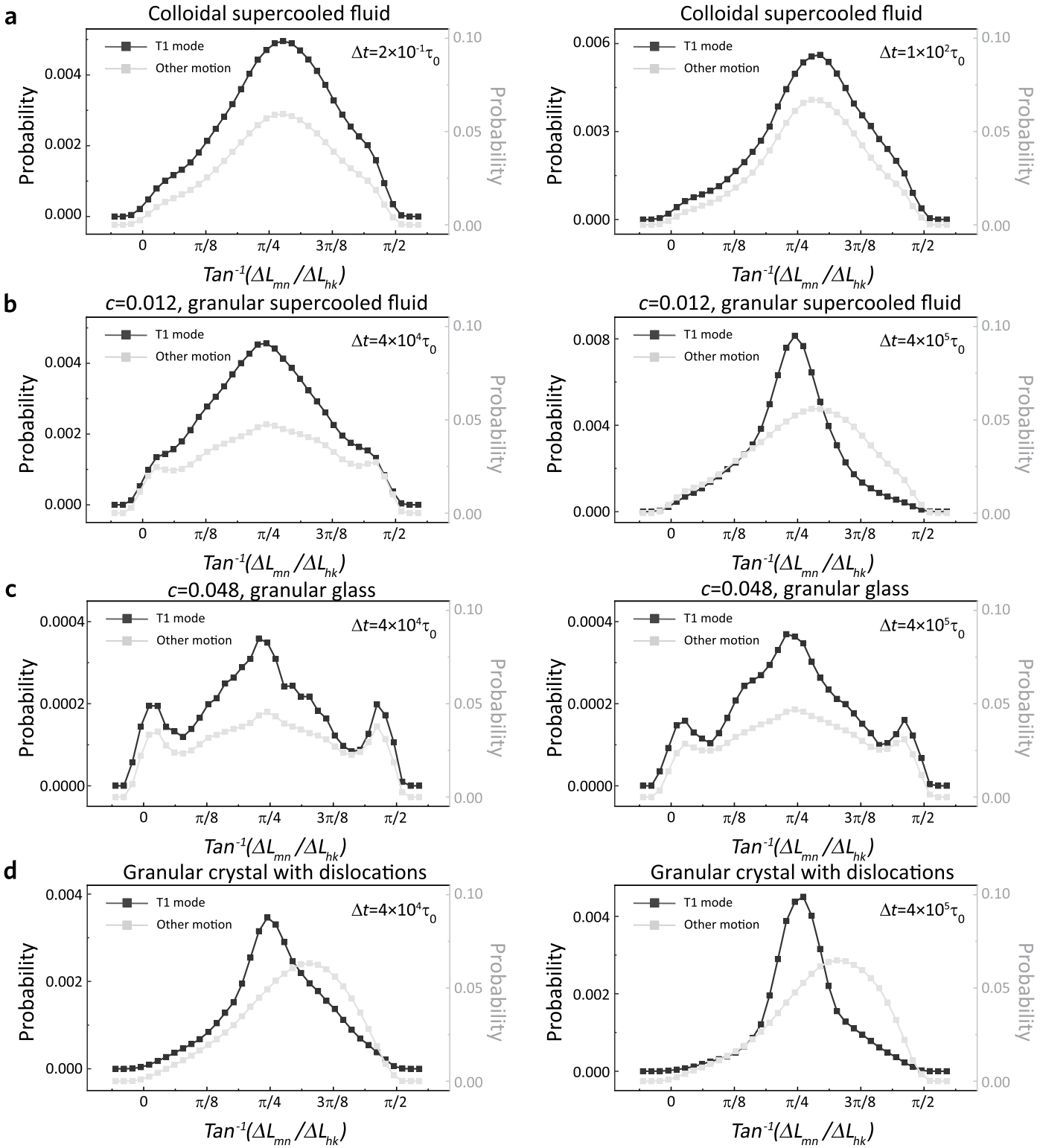

Extended Data Fig. 8 | Probability distribution of $tan^{-1}(\Delta L_{m,n}/\Delta L_{h,k})$ for the two glass and crystalline systems with dislocations. a, A strong signature of FM is observed, whereas RM is absent in the supercooled colloidal liquid with short-range interactions that represents fast-β (left panel) and α (right panel) modes. **b**, The deeply supercooled granular liquid sample with long-range soft interaction that represents slow-β and α modes (c ~ 1.2%). We find a weak signature of RM for slow-β relaxation (middle panel), whereas RM is absent for early-α relaxation (right panel). **c**, The granular glass sample with long-range soft interaction that represents slow-β mode (c ~ 1.2%). We find a strong signature of RM when early-α relaxation is absent. **d**, The granular, crystalline system with dislocations. Both RM and small-T1 events are absent. We find a strong signature of $\Delta L_{m,n}/\Delta L_{h,k} \sim \sqrt{3}$, indicating the elastic nature. The results shown here correspond to those in Extended Data Fig. 6.